



**HAL**  
open science

## **SCIAMACHY Level 1 data: calibration concept and in-flight calibration**

G. Lichtenberg, Q. Kleipool, J. M. Krijger, G. van Soest, R. van Hees, L. G. Tilstra, J. R. Acarreta, I. Aben, B. Ahlers, H. Bovensmann, et al.

► **To cite this version:**

G. Lichtenberg, Q. Kleipool, J. M. Krijger, G. van Soest, R. van Hees, et al.. SCIAMACHY Level 1 data: calibration concept and in-flight calibration. Atmospheric Chemistry and Physics, 2006, 6 (12), pp.5347-5367. hal-00296084

**HAL Id: hal-00296084**

**<https://hal.science/hal-00296084>**

Submitted on 18 Jun 2008

**HAL** is a multi-disciplinary open access archive for the deposit and dissemination of scientific research documents, whether they are published or not. The documents may come from teaching and research institutions in France or abroad, or from public or private research centers.

L'archive ouverte pluridisciplinaire **HAL**, est destinée au dépôt et à la diffusion de documents scientifiques de niveau recherche, publiés ou non, émanant des établissements d'enseignement et de recherche français ou étrangers, des laboratoires publics ou privés.

## SCIAMACHY Level 1 data: calibration concept and in-flight calibration

G. Lichtenberg<sup>1,\*\*</sup>, Q. Kleipool<sup>1,\*</sup>, J. M. Krijger<sup>1</sup>, G. van Soest<sup>1,2</sup>, R. van Hees<sup>1</sup>, L. G. Tilstra<sup>2</sup>, J. R. Acarreta<sup>2</sup>, I. Aben<sup>1</sup>, B. Ahlers<sup>4</sup>, H. Bovensmann<sup>3</sup>, K. Chance<sup>6</sup>, A. M. S. Gloudemans<sup>1</sup>, R. W. M. Hoogeveen<sup>1</sup>, R. T. N. Jongma<sup>1</sup>, S. Noël<sup>3</sup>, A. Piters<sup>2</sup>, H. Schrijver<sup>1</sup>, C. Schrijvers<sup>4,\*</sup>, C. E. Sioris<sup>6</sup>, J. Skupin<sup>3,\*\*\*</sup>, S. Slijkhuis<sup>5</sup>, P. Stammes<sup>2</sup>, and M. Wuttke<sup>3</sup>

<sup>1</sup>SRON National Institute of Space Research, Utrecht, The Netherlands

<sup>2</sup>Royal Netherlands Meteorological Institute (KNMI), de Bilt, The Netherlands

<sup>3</sup>Institute of Remote Sensing (IfE), University of Bremen, Germany

<sup>4</sup>TNO Science and Industry, Delft, The Netherlands

<sup>5</sup>DLR-DFD/IMF, Weßling, Germany

<sup>6</sup>Harvard-Smithsonian Center for Astrophysics (SAO), Cambridge, USA

\* now at: Royal Meteorological Institute Netherlands (KNMI), de Bilt, The Netherlands

\*\* now at: DLR-DFD/IMF, Weßling, Germany

\*\*\* now at: Deutsches Elektronen-Synchrotron (DESY), Notkestr. 85, 22607 Hamburg, Germany

Received: 11 April 2005 – Published in Atmos. Chem. Phys. Discuss.: 19 September 2005

Revised: 5 October 2006 – Accepted: 18 November 2006 – Published: 28 November 2006

**Abstract.** The calibration of SCIAMACHY was thoroughly checked since the instrument was launched on-board ENVISAT in February 2002. While SCIAMACHY's functional performance is excellent since launch, a number of technical difficulties have appeared, that required adjustments to the calibration. The problems can be separated into three types: (1) Those caused by the instrument and/or platform environment. Among these are the high water content in the satellite structure and/or MLI layer. This results in the deposition of ice on the detectors in channels 7 and 8 which seriously affects the retrievals in the IR, mostly because of the continuous change of the slit function caused by scattering of the light through the ice layer. Additionally a light leak in channel 7 severely hampers any retrieval from this channel. (2) Problems due to errors in the on-ground calibration and/or data processing affecting for example the radiometric calibration. A new approach based on a mixture of on-ground and in-flight data is shortly described here. (3) Problems caused by principal limitations of the calibration concept, e.g. the possible appearance of spectral structures after the polarisation correction due to unavoidable errors in the determination of atmospheric polarisation. In this paper we give a complete overview of the calibration and problems that still have to be solved. We will also give an indication of the

effect of calibration problems on retrievals where possible. Since the operational processing chain is currently being updated and no newly processed data are available at this point in time, for some calibration issues only a rough estimate of the effect on Level 2 products can be given. However, it is the intention of this paper to serve as a future reference for detailed studies into specific calibration issues.

### 1 Introduction

SCIAMACHY (SCanning Imaging Absorption spectroMeter for Atmospheric CHartography) is a scanning nadir and limb spectrometer covering the wavelength range from 212 nm to 2386 nm in 8 channels (see Table 1). It is a joint project of Germany, the Netherlands and Belgium and was launched in February 2002 on the ENVISAT platform. The nominal mission life time of ENVISAT is 5 years. SCIAMACHY was designed to measure column densities and vertical profiles of trace gas species in the mesosphere, in the stratosphere and in the troposphere (Bovensmann et al., 1999). It can detect O<sub>3</sub>, H<sub>2</sub>CO, SO<sub>2</sub>, BrO, OClO, NO<sub>2</sub>, H<sub>2</sub>O, CO, CO<sub>2</sub>, CH<sub>4</sub>, N<sub>2</sub>O, O<sub>2</sub>, (O<sub>2</sub>)<sub>2</sub> and can provide information about aerosols and clouds. In addition to the spectrally resolved measurements of the radiance reflected from the Earth's atmosphere, the polarisation of the

Correspondence to: G. Lichtenberg  
(guenter.lichtenberg@dlr.de)

incoming light is measured with 7 broadband sensors. In this paper we describe the optical layout of SCIAMACHY, its different observation modes and the on-ground and in-flight calibration concept. We also cover unexpected calibration problems encountered in-flight that require adjustments in the data processing.

During the on-ground calibration the polarisation sensitivity and the radiometric sensitivity was extensively measured for a range of scanning angles. A dedicated on-board calibration unit that contains a White Light Source (WLS) and a Spectral Line Source (SLS) allows monitoring the instrument during the whole mission. Solar measurements are additionally employed to measure light path degradation (see Noël et al., 2003).

All calibration and science data are linked down to ESA ground stations where they are further processed under responsibility of ESA. The user is provided with two types of SCIAMACHY data: (1) Level 1 data, which contain the spectrum, polarisation fractions and other information and (2) Level 2 data containing geophysical products like total columns or profiles of atmospheric trace gases. Level 1 data are generated from raw, uncorrected Level 0 data and are split up in Level 1b and Level 1c data. Level 1b data are still uncalibrated, but contain all the necessary information to do a full calibration. Level 1c data are produced by applying some (or all) calibration steps to Level 1b data. ESA provides a tool to calibrate Level 1b data, but the user can also use third party software or develop dedicated software to calibrate the data. Often in this paper we will speak of “operational” data processing as opposed to “scientific” processing. Operational data processing is done by ESA and/or is using official ESA tools, while scientific data products are products that scientists have developed themselves. An example for scientific processing is a software package developed at SRON that produces fully calibrated Level 1c data and already incorporates some of the corrections that will become available operationally only after an update of the ESA data processor. Many scientific Level 2 products have been developed by different research groups at IfE, KNMI, IUP Heidelberg, SRON and other institutes. The operational processor was mainly developed by DLR-IMF in collaboration with ESA.

The operational data processing is currently (spring 2005) being updated from the previous version (5.04) to include the latest calibration algorithms and key data. The implementation of this new calibration will be checked and – if necessary – be adjusted until end 2005. After the revision of the data processing, all data will be re-processed with the new processing chain. Excluded from the current update are important corrections for the IR detectors (see below), partly because no operational algorithm is available at this point in time and partly because other corrections were set at a higher priority. Without these corrections operational products from the IR wavelength range will be of lower quality and users must develop their own retrieval algorithm or must

make use of trace gas products developed in the scientific community (e.g. Buchwitz et al., 2005; Gloudemans et al., 2005; Frankenberg et al., 2005).

The paper is organised as follows: the first section describes the different instrument modes and the layout of the instrument. Then the overall calibration concept is discussed in the second section before the individual calibration steps are explained in Sects. 3–7. Section 8 treats unexpected effects that require an adjustment of the calibration procedure such as ice in channels 7 and 8 and the light leak in channel 7. Finally, in Sect. 9, a summary of the most important open calibration issues is given.

## 2 The instrument

SCIAMACHY has various observation modes to obtain spectra from the Earth’s atmosphere, the sun and the moon. Two scanner modules, the so-called Elevation Scanner Module (ESM) and Azimuth Scanner Module (ASM) can be used to direct light into the instrument. Both scanner modules can be rotated a full 360° and have identical flat, uncoated mirrors mounted on one side and a diffuser mounted on the other side. The scanners enable SCIAMACHY to perform observations in the following modes (see also Noël et al., 2002):

*Nadir:* The instrument is looking directly down to the Earth and uses only the ESM mirror. The Instantaneous Field of View (IFoV) is approximately 25 km×0.6 km (along × across track), the typical ground pixel size is 32 km×60 km at a full swath width of 960 km (scanning East–West). Higher spatial resolution is possible in special operation modes.

*Limb:* The instrument looks into flight direction using the ASM mirror for East–West scans and the ESM mirror to sample heights from the horizon to an altitude of 93 km in 3 km steps. The IFoV is 103 km×2.6 km (azimuth × elevation) at the tangent point around 3000 km ahead of the satellite. The typical spatial resolution is 240 km×3 km covering 960 km in one East–West scan. The ESM scanner compensates for the curvature of the Earth to keep the same tangent height for each individual East–West scan. At the end of each Limb measurement a dark signal measurement is made at a tangent height of 250 km.

*Solar Occultation:* The sun is tracked, starting at sunrise over the Northern Pole and is followed through the atmosphere from 17 km to the upper edge of the atmosphere. In this observation mode the small aperture is inserted into the optical path to reduce the signal in all channels. Additionally, the Neutral Density Filter (NDF) reduces the light in channels 3–6 by a factor of about 5.

*Solar Irradiance:* In this observation mode a solar spectrum is measured with a mirror diffuser combination (either ASM mirror + ESM diffuser + NDF filter or ASM diffuser + ESM mirror) to obtain a solar reference spectrum.

**Lunar Occultation:** Similar to the solar occultation mode, the moon is tracked through the atmosphere in this mode. However, due to the orbit of ENVISAT and the revolution of the moon, lunar observations are only possible at certain times over the North or South Pole. Since in the Northern hemisphere the sun and moon rise coincide, observations are only made when ENVISAT is in the Southern hemisphere. Here the moon is visible once per month for a time period of approximately a week (depending on season). The phase of the moon varies between 0.6 and 1 during the week of observations. The NDF and the small aperture are not needed in this observation mode.

**Monitoring:** In this mode the sun or the moon are observed above the atmosphere in order to measure any degradation of the instrument optical path. In the sun modes the small aperture and the NDF is used. The sun can be observed with both mirrors (Limb configuration), in Limb configuration with an extra mirror in front of the Nadir mirror or in the so-called sub-solar mode using only the Nadir mirror. Sub-solar measurements are only possible when the satellite crosses the equator on the day side. The extra mirror is used to determine the degradation of the ESM mirror. It is protected when not employed and it is assumed that it will not degrade significantly during the mission.

**Calibration:** SCIAMACHY has a dedicated calibration unit with a 5 Watt Tungsten halogen WLS for instrument monitoring and a PtCrNe spectral line source (SLS) to perform in-flight spectral calibration. Both lamps can be observed only with the ESM (mirror or diffuser).

A simplified optical train for all possible observation modes is shown in Fig. 1. After passing the scanners a 31 mm diameter telescope mirror produces a focus on the entrance slit of the spectrometer. The entrance slit is 180  $\mu\text{m}$  wide and 8 mm high, resulting in an Instantaneous Field of View (IFoV) of 0.045 degrees in the dispersion direction and 1.88 degrees in the cross-dispersion direction. After the slit the beam is collimated and is directed into the Optical Bench Module (OBM).

The OBM design is based on the double dispersing spectrometer principle. The light is first dispersed by a pre-disperser prism creating an intermediate spectrum. Small pick-off prisms and subsequent dichroic mirrors direct the light into the 8 so-called science channels. Each of these channels contains a grating for the final dispersion of the light to moderate spectral resolution. At the pre-disperser prism p-polarised light is split off to the Polarisation Measurement Devices (PMDs) through a Brewster reflection. The PMDs are broadband sensors with wavelength ranges that cover approximately the wavelengths measured in channels 2–6 and 8 (see Table 1). Additionally to the 6 PMDs A–F measuring Q the PMD 45 measures the U Stokes parameter. The PMDs are non-integrating devices that are read out at 40 Hz. The polarisation of the incoming light can be derived by combining the measurements in the science channels and the PMD

**Table 1.** Spectral characteristics of the science channels and the PMDs. The detector temperature values are the approximate minimum and maximum value from the year 2004 excluding periods when the detectors are heated for decontamination purposes. The PMD wavelength range is defined such that it contains 80% of the signal, the range of the science channels is the total range.

Ch.	Wavelength range [nm]	Resolution [nm]	Temperature Det. [K]	PMD	Wavelength range [nm]
1	212–334	0.24	205.8–207.5	–	–
2	300–412	0.26	205.0–207.0	A	310–365
3	383–628	0.44	224.0–225.0	B	455–515
4	595–812	0.48	223.0–224.3	C	610–690
5	773–1063	0.54	221.4–222.4	D/45	800–900
6	971–1773	1.48	199.0–201.2	E	1500–1635
7	1934–2044	0.22	145.0–149.0	–	–
8	2259–2386	0.26	143.7–147.6	F	2280–2400

measurements as will be explained in Sect. 7.

The science channels of SCIAMACHY employ two types of detectors. For the UV/VIS range (channels 1–5) standard silicon EG&G Reticon detectors with 1024 pixels are used. The pixels are sequentially read out in approximately 30 ms for the complete array. The near IR channels 6–8 employ Indium Gallium Arsenide (InGaAs) detectors manufactured by EPITAXX (now owned by JDS Uniphase). The focal plane array for these channels was designed and built by SRON (Hoogeveen et al., 2001). All 1024 pixels of the IR detectors are read out in parallel with dedicated amplifiers. In order to cover the whole wavelength range from 971 to 2386 nm, the composition of the IR detector material had to be adjusted leading to side effects important for the calibration: The InGaAs light detecting layer of the IR detectors is epitaxially grown on an InP substrate. For optimal detector performance, the lattice constant of the InGaAs layer and the InP substrate must match. Ideal lattice matching between detector and substrate material occurs for 53% Indium and 47% Gallium only. Detectors with this composition are sensitive only up to wavelengths of 1600 nm at 200 K. For sensitivity beyond this wavelength, a higher Indium and lower Gallium content is needed. The composition of the detector material in channels 6+ (pixels 794–1023 in channel 6), channel 7 and channel 8 was changed accordingly. However, this results in a larger lattice constant and thus in a mismatch with the lattice constant of the InP substrate. Therefore, these channels have a reduced performance in terms of detector dark current, noise and number of usable pixels (see Sect. 4.2).

The sequential readout of the individual pixels in channels 1–5 leads to an effect called spatial aliasing: Pixels that are read out at a different time see a different ground scene because of the movement of the satellite and the scan mirrors, introducing a wavelength dependent bias into the spectrum. The magnitude of the effect depends on the variability of the ground scene. In order to reduce spatial aliasing in the

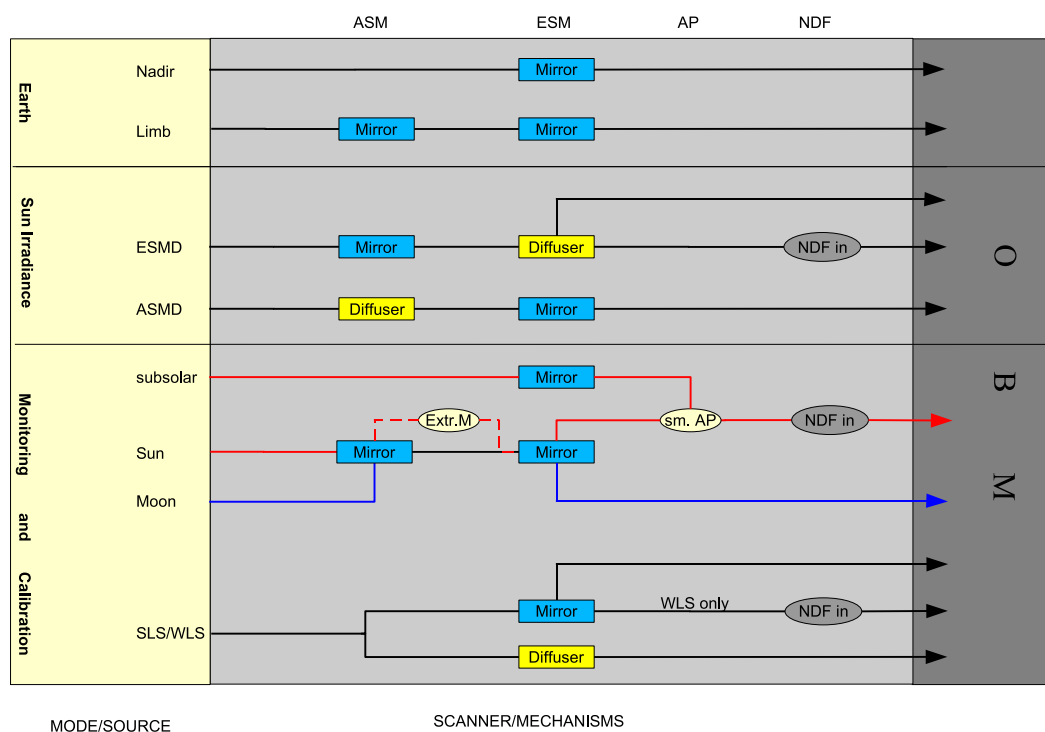


**Fig. 1.** Simplified optical train of SCIAMACHY for the different observation modes. Only elements not common to all paths are shown. Note that the NDF is only in the light path of channels 3–6. Mirrors are marked blue, diffusers yellow. The optical path in the monitoring mode for the sun is marked red, the path for the moon is marked blue, “sm. AP” denotes the small aperture, “Extr. M” the extra mirror that can be put into the light path optionally.

overlap of channel 1 and channel 2 from 300–334 nm and in the overlap of channels 2 and 3 (383–412 nm) the wavelength direction in channel 2 is reversed, i.e. *high* pixel numbers correspond to *short* wavelengths. This ensures that the channel overlaps between consecutive channels observe the same ground scene. Channels 6–8 pixels are – as mentioned earlier – read out in parallel and thus do not suffer from spatial aliasing.

The scanning motion of the mirrors and the readout of the detectors are synchronised by pulses with a frequency of 16 Hz (corresponding to 62.5 ms). Since the time needed for the readout of all 1024 pixels of the UV/VIS channels is 28.78 ms, the minimum exposure time of the detectors is set to  $62.5 \text{ ms}/2 = 31.25 \text{ ms}$  to allow for a proper synchronisation. The IR channels 6–8 can also be read out in the so-called “hot mode” allowing much shorter integration times of down to  $28 \mu\text{s}$ . However, in measurements with integration time shorter than the synchronisation time of 62.5 ms all readouts except one are discarded i.e. not sent to the ground station. For example, in a measurement with 31.25 ms integration time only every second readout is actually available in the data product. Integration times shorter than 62.5 ms are only used in calibration and monitoring modes.

In order to reduce the noise on the signal, the detectors are cooled by a dual-stage, passive radiative cooler (SCIAMACHY Radiative Cooler, SRC). The first stage provides cooling to channels 1–6 and the second stage to channels 7 and 8. Seasonal variations of the detector temperature are compensated by manual adjustment of the power to three so-called trim heaters. Channels 6+, 8 and 5 (in decreasing order of sensitivity) show a significant temperature dependence of their quantum efficiency. The responses of those detectors changes up to 2–3% per Kelvin depending on the wavelength. Table 1 shows the approximate detector temperature range for the year 2004, excluding decontamination periods. The temperature of the optical bench is actively controlled by a feed-back loop holding the temperature stable at  $255.251 \text{ K} \pm 40 \text{ mK}$  over one complete orbit. The remaining temperature variation over the orbit leads to a small change of the background signal in channel 8 (see Sect. 4.2).

Finally, a special feature of the readout of the detectors has to be mentioned. The total integration time in a channel is defined as the product of the Pixel Exposure Time (PET) and a co-adding factor. The detectors are always read out after the time specified in the PET parameter. The co-adding factor determines how many readouts are summed up before the data are sent to the ground station. If the co-adding factor

is larger than 1, the individual readouts are not available in the data product, only the sum of the readouts is. It is possible to assign consecutive pixels to so-called clusters, each having its own co-adding factor, i.e. the integration time in each cluster can be a multiple of the PET in a given channel. Only one PET value per channel is possible<sup>1</sup>. The cluster definition can be tuned such that the spatial resolution in the spectral windows containing the most important trace gases is the highest. In this way the scientific return can be optimised within the limits of the data rate that is available to SCIAMACHY for downlinking the data. A drawback of this concept is that it introduces several complications in the data processing of SCIAMACHY. The different integration times of the clusters mean that not the complete spectrum is available for every record in the data. If, for example, we have two clusters A and B in a channel and cluster A has an integration time two times larger than the integration time of cluster B, then a full spectrum containing data from both clusters is only available in every second record of the data. Generally, a full spectrum over a channel is available in the data only for the longest integration time of the channel (since only then all clusters of the channel have been read out). The same is true for the complete spectrum over the whole spectral range of SCIAMACHY, only that this is available after the longest integration time of *all channels*. The observation mode, the cluster definition and the integration time setting for the channels constitute what is called a “state”. SCIAMACHY has 70 pre-defined states that cover all Earth observation, monitoring and calibration modes.

### 3 Calibration concept

The calibration aims to convert electronic signals of the detectors (Binary Units/second) into physical units (e.g. W/m<sup>2</sup>/nm/sr). The general calibration formula is

$$S_{\text{det}} = I(\lambda) \cdot \Gamma_{\text{inst}}(\lambda) \cdot QE(T_{\text{det}}, \lambda) + S_{\text{stray}} + DC + S_{\text{elec}}(1)$$

where  $S_{\text{det}}$  is the signal measured on the detector in Binary Units/second,  $I$  is the incoming intensity,  $\Gamma_{\text{inst}}$  the total transmission of the instrument,  $QE$  the quantum efficiency,  $S_{\text{stray}}$  the stray light,  $DC$  the total dark signal and  $S_{\text{elec}}$  electronic effects like non-linearity. This equation must be solved for every detector pixel. In order to obtain the spectrum as a function of wavelength  $\lambda$ , the wavelength has to be determined for each pixel and the equation has to be inverted to calculate the intensity  $I$ . Additionally, to get the true shape of the spectrum the instrument specific slit function has to be applied. The transmission of the instrument is dependent on the polarisation of the incoming light. The individual calibration steps to obtain the spectrum will be explained in more

detail in the following sections. First the general concept behind the calibration of the SCIAMACHY instrument is discussed.

The experience of the Global Ozone Monitoring Experiment (GOME), launched on-board the ERS-2 satellite in 1995, where various air-vacuum effects led to calibration problems, showed that spectrometers should ideally be calibrated under thermal vacuum (T/V) conditions (see e.g. Aben et al., 2000). In the case of SCIAMACHY, a calibration performed completely under T/V conditions was not possible, because the range of incidence angles on the mirror(s) and mirror-diffuser combination that had to be covered could not be realised in the available vacuum tank. Therefore a combination of T/V and ambient measurements was used. The radiometric sensitivity and the polarisation sensitivity of the instrument were measured under T/V conditions for *one* reference angle  $\alpha_0$  and all necessary instrument modes (limb, nadir and irradiance). In order to be able to calibrate all incidence angles on the mirrors (or diffusers), component level measurements of all possible mirror combinations and the mirror-ESM diffuser combination were made under ambient conditions. In the component level measurements only the scanner modules with the mirror and diffuser are mounted on an optical table that allows to orient the mirror (combination) at arbitrary angles w.r.t. to the calibration light source and each other. The reflectivity of the components is then measured using a dedicated detector different from the ones used in SCIAMACHY. These ambient measurements were performed for a selected set of angles (including  $\alpha_0$ ) and wavelengths. The reference angle measurement is used to transfer the results from the ambient measurement to the T/V measurement. Measurements were done for unpolarised light, s- and p-polarised light and  $\pm 45^\circ$  polarised light. The combination of T/V measurements and ambient measurements provides ideally the correct instrument response for all incidence angles at begin of life of the instrument. The implicit assumptions for the combination of the T/V and ambient measurements are that the polarisation dependence of the mirrors and diffusers are the same in air as they are in vacuum and that there is no temperature dependence. Both assumptions are reasonable for SCIAMACHY, since uncoated mirrors are used. Critical points in the transfer of ambient to T/V measurements are the geometry (incidence angles on the mirrors or diffusers), the illumination conditions and the detector used in the component measurements. Obviously, errors in the geometry lead to a wrong angle dependence of the calibration quantity to be measured. The illumination during instrument measurements and during component measurements will always be different. While the footprint of the light source on the component can be matched to the footprint during the instrument measurements, it is impossible to re-create the exact illumination conditions potentially leading to systematic errors in the calibration. Finally, care has to be taken that the detector used in the ambient measurements does not introduce artifacts. In order to minimise

<sup>1</sup>Channels 1 and 2 are divided in two parts w.r.t. PETs, i.e. for these channels 2 different PETs, one for each part, are possible.

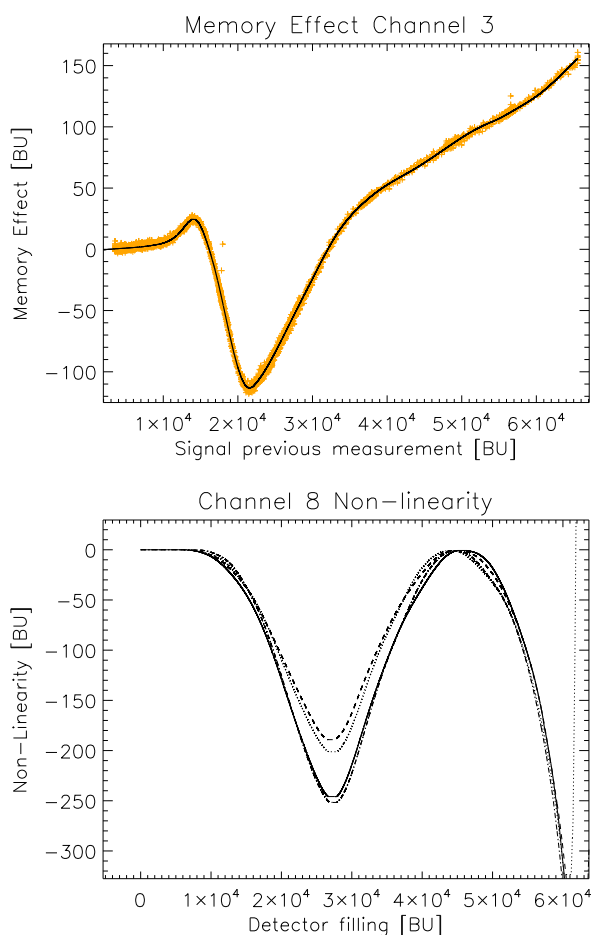


**Fig. 2.** Top: Memory Effect in channel 3 as a function of the detector signal of the previous readout. Shown is an in-flight measurement from July 2003 (orange crosses) and a spline fit through the data (solid line). Bottom: Non-linearity for channel 8: low odd pixels (solid), low even pixels (dashed), high odd pixels (dot-dashed) and high even pixels (dotted).

possible errors in ambient measurements, only ratios of measurements were used in the ambient calibration where possible.

In addition to the on-ground calibration measurements, in-flight measurements of the dark signal are performed in every orbit. Changes of the instrument performance in-flight are tracked with internal light sources (WLS and SLS) and solar measurements. For more details on monitoring see e.g. Noël et al. (2003). Details of the calibration are described in the following sections.

#### 4 Detector corrections

This section describes corrections related to the electronics of the detectors and the detectors themselves ( $S_{elec}$  and  $DC$  in Eq. 1). The UV/VIS channels 1–5 and the IR chan-

nels 6–8 have to be treated separately in the calibration due to the differences in detector material and readout electronics. The signal in this section is described in terms of Binary Units (BU). The Analog-to-Digital Converter (ADC) of SCIAMACHY codes the signal on the detector in 16 bit meaning that detector signals (or “fillings”) are in the range between 0 BU and 65 535 BU.

##### 4.1 Channels 1–5 (UV/VIS)

###### 4.1.1 Memory effect

The first correction that has to be applied is the so-called memory effect (see e.g. Lichtenberg, 2003). The memory effect was discovered in 1996 during an investigation of the linearity of channels 1–5. In a number of measurements that covered the range from low detector fillings to saturation it was found that the signal deviated from a linear response<sup>2</sup>. The deviation was not dependent on the actual signal level, but on the signal level of the previous readout (hence the name memory effect). Note that the effect depends on the signal level including the analog offset (see below) and dark current. Thus it is the first correction to be applied. In order to characterise the memory effect, WLS measurements followed by several dark measurements were done on-ground and in-flight. The difference between the first dark measurement after the WLS measurement and subsequent dark measurements gives a correction value as a function of detector filling. This value has to be subtracted from the data to correct for the memory effect. The memory effect is the same for all pixels. The total correction for a single readout is – depending on the channel – between –0.61% and 0.21% of the detector filling of the previous readout with a maximum effect at fillings around 19 000 BU–21 000 BU (see Fig. 2). Since the memory effect introduces instrument features that depend on the previous readout, it is not easily possible to make a quantitative estimate of the effect on scientific data. Qualitatively, the memory effect leads to two different kinds of deviations from the “true” spectrum. First, the absolute value of the signal will be wrong, but for measurements that have a reasonable S/N this is not considered a major problem. The second effect, however, is more serious. Since the memory effect changes rapidly as a function of the previous signal for a large range of detector fillings, there is a risk that artificial spectral features are introduced into the measurements. Differential retrieval methods, such as Differential Optical Absorption Spectroscopy or DOAS (see e.g. Solomon et al., 1987; Platt, 1994; Burrows et al., 1999) are very sensitive to changes of the spectral shape of a line, thus the memory effect cannot be neglected. In general the effect on the data is strongest when for a certain spectral region the previous readout had detector fillings that lead to a large memory effect and the current readout has a very weak signal or when

<sup>2</sup>Defined by doing a linear fit for all points of up to 90% of the maximum detector filling.

the spectrum shows a high variability in signal levels (e.g. partially clouded scenes on a dark background like ocean).

In three cases the memory effect cannot be calculated directly from the available data in a channel. First, if the data are co-added, the individual detector readouts are not available. In this case PMD measurements, which are read out more frequently than the science channels, are used to estimate the signal in the science channels during the individual readouts in a co-adding sequence. The estimated signals are then used to approximate the total memory effect. Second, each time the instrument changes into a different state (see Sect. 2 for the definition of a state) the mirrors move first into an idle position and then into the position required by the new state. During the movement to the new position the detectors are continuously read out, picking up an arbitrary signal from the moving mirror. Data obtained while the mirrors are still moving are dumped on-board. Thus the previous readout for the first spectrum in a state is not available. The operational processor uses some approximation to estimate the signal during mirror movement, but it is impossible to determine how accurate this approximation is. For this reason it is recommended not to use the first readout in a state or, if one does so, carefully inspect the spectrum for artifacts. The third case is the Limb observation mode: Before each observation of a new tangent height there is a so-called “reset readout” of the detectors with an integration time of 31.25 ms, which is not linked down to the ground station. The signal of the reset readout is estimated using the Limb measurements itself and then applied to the first readout at the new tangent height.

#### 4.1.2 Dark correction

The second detector correction that has to be applied is the dark signal correction. The dark signal is measured in every orbit in the eclipse using 5 different states. In channels 1–5 two components contribute to the dark signal: the analog offset (AO) and the leakage current (LC). The analog offset is independent of integration time, it is just a fixed signal added to the measured signal to avoid negative values. The leakage current is caused by thermally created electron-hole pairs. The total dark signal for the UV/VIS channels is

$$DC_{UV/VIS} = f_{\text{coadd}} \cdot AO + f_{\text{coadd}} \cdot t_{\text{PET}} \cdot LC \quad (2)$$

where  $f_{\text{coadd}}$  is the co-adding factor of the cluster and  $t_{\text{PET}}$  is the pixel exposure time (see Sect. 2). Note that the analog offset is multiplied with the co-adding factor since it is added to the signal for every individual detector readout. The dark signal correction is derived in-flight by a linear fit to the dark measurements with different integration times. The dark signal in the UV/VIS channels is dominated by the analog offset. The leakage current is only 0.04–0.5 BU/s (Kleipool, 2002) and did not change significantly since launch.

## 4.2 Channels 6–8 (IR)

### 4.2.1 Non-linearity

The IR channels do not suffer from the memory effect. However, there is a significant non-linearity that has to be corrected before applying other corrections. The non-linearity has been measured during the on-ground calibration campaign and a correction algorithm was defined (Kleipool, 2003). The maximum non-linearity is around 250 BU, which can be significant for weak absorbers like CO. A non-linearity correction has been derived for each of the channels 6, 6+, 7 and 8 separately. Within these channels the non-linearity differs for odd and even pixels because they are connected to different multiplexers. Additionally there is a clear difference in the non-linearity between pixels with numbers higher and lower than 511. This leads to a total of 14 correction curves, four per channel with the exception of channel 6+, which covers only pixels 794 to 1024 (see Sect. 2). Figure 2 shows the non-linearity curves derived for channel 8. The accuracy of the non-linearity correction is around 5–21 BU for detector fillings in the range from 10 000 to 40 000 BU, depending on the channel.

### 4.2.2 Bad and dead pixels

In addition to the non-linearity, Channels 6+, 7 and 8 contain a significant number of pixels with reduced performance due to the lattice mismatch between the light detecting InGaAs layer and the InP substrate. These pixels are called bad or dead pixels. There are various effects that make these pixels unusable: a few are disconnected, thus preventing any signal readout. Some pixels are so-called Random Telegraph (RT) pixels that spontaneously and unpredictably jump between two or more levels of dark current leading to different detected signals for the same intensity. Other effects include excessive noise or too high leakage current leading to saturation of the detector. All these effects were measured on-ground and a so-called Bad and Dead pixel Mask (BDM) was created. Pixels in the BDM have to be ignored in any retrieval. Recently it has been discovered that the BDM changes in-flight. The most likely reason is the impact of high energy protons on the detector (Kleipool et al., 2006). The effect of the changes of the BDM on CH<sub>4</sub> and CO is described in detail by Gloudemans et al. (2005). It is demonstrated that one bad pixel that is not included in the BDM can change the CH<sub>4</sub> retrieved total columns by a factor of up to 2. Clearly, the effect on individual retrievals depends on the position of the bad pixel in the retrieval window and on the used retrieval algorithm.

### 4.2.3 Dark correction

After application of the non-linearity and the BDM, the dark signal has to be corrected. The dark signal correction in channels 7 and 8 is complicated by the presence of a

large thermal background signal ( $BG_{th}$ ) and the unforeseen growth of an ice layer on the detector (see Sect. 9.1). The ice layer slowly changes the detector temperature and attenuates the signal on the detector, including the thermal background. The dark signal in these channels becomes

$$DC_{IR} = f_{coadd} \cdot AO + f_{coadd} \cdot t_{PET} \cdot LC + f_{coadd} \cdot t_{PET} \cdot \Gamma_{ice}(\lambda, t) \cdot QE(T_{det}, \lambda) \cdot BG_{th}(\varphi) \quad (3)$$

where  $\Gamma_{ice}$  is the transmission coefficient of the ice layer and  $QE$  is the quantum efficiency of the detector. For channels 6+ and 8 the quantum efficiency varies with detector temperature  $T_{det}$ , whereas the first part of channel 6 and channel 7 show no significant temperature dependence. The thermal background is caused by the thermal radiation emitted by the instrument and is the dominant part of the dark signal ( $\approx 4000$  BU/s) in channel 8. The thermal background signal depends on the orbit phase  $\varphi$ , because the temperature of the instrument is not completely stable, but varies over one orbit due to the changing angle of the solar irradiation. The variation of the dark signal can be up to 60 BU/s which has significant impact on the retrievals of trace gases. Gloude-mans et al. (2005) showed a comparison of retrievals with and without correction of the orbital variation results in differences of up to 4% in  $CH_4$  total columns. The orbital variation of the dark signal is measured once a month during a special calibration orbit in which only dark signal measurements are performed by looking to 250 km tangent height in Limb mode. Discussions are under way on how to best implement the orbital variation in the operational processing. The variation of the transmission makes the dark signal correction time dependent meaning that for the channels 7 and 8 a dark signal correction calculated from measurements in the same orbit has to be used.

#### 4.2.4 Pixel-to-Pixel Gain (PPG)

The final detector related correction is the PPG correction. The pixels in the IR detectors do not show the same, uniform response to the incoming light as observed in the UV/VIS channels. Variations of a few percent can be observed from pixel to pixel. The PPG is derived by first smoothing a WLS measurement, assuming the spectrum is flat. Then the original spectrum is divided by the smoothed measurement, leaving only the high frequent variations that are caused by the different pixel gains in the result, which can then be used to correct the PPG. Preliminary investigations by SRON show that the PPG is very stable since launch (R. Jongma, private communication, 2005). It is important to realise that the PPG is an effect that is caused by combined effects of the electronics and the detector and is thus only associated with the individual pixel and not with the wavelength. One example where this becomes an issue is the calculation of the Earth reflectance by dividing it by a sun spectrum. The spectrum of the sun is slightly Doppler shifted due to the movement of

the satellite relative to the sun. The PPG correction has to be applied before the Doppler shift is corrected.

## 5 Wavelength calibration

The spectral calibration of the SCIAMACHY data is regularly updated using in-flight data with the exception of channels 7 and 8 (see below). In order to determine the exact wavelength value for each pixel a combination of a *basis wavelength calibration* and an in-flight wavelength calibration is used. The basis wavelength calibration is determined from on-ground data. The in-flight calibration calculates only the difference to the basis wavelength calibration. This has the advantage that only a small correction has to be applied, because it is expected that the wavelength calibration of SCIAMACHY is relatively stable over the mission lifetime. The small correction can be modelled with a lower order polynomial function avoiding the problem of oscillations possible for higher order polynomial fits, especially at the channel edges. In the in-flight calibration the pixel position of selected lines is determined using the Falk algorithm (Falk, 1984). The pixel positions are then used together with the basis wavelength calibration and the theoretical line positions to determine the wavelength of each pixel (for details see Slijkhuis, 2000). Measurements of solar Fraunhofer lines are used as a quality check.

On-ground, the wavelength calibration was performed both with the internal SLS and an external SLS. However, for channels 7 and 8 not enough useful lines are available to calculate the wavelength calibration with a sufficient accuracy. In channel 8 this is caused by bad pixels that interfere with the determination of the line position. Channel 7 only contains two strong doublet lines preventing an accurate determination of line positions over the whole channel. In both channels data from on-ground gas cell absorption measurements are used to establish the wavelength calibration. This calibration is also used for in-flight data, i.e. the wavelength calibration is not updated regularly in-flight. In the future it might be possible to update the calibration using sun, moon or Earth (ir)radiance spectra.

As mentioned above, during the on-ground calibration the internal SLS of SCIAMACHY and an external SLS was used to check the wavelength calibration. A comparison between the external and internal spectral lamp measurements revealed a wavelength shift of up to 0.07 nm. The shift is explained by a partial blocking of the light path during internal SLS measurements. This so-called “blocking shift” was characterised and is corrected when the wavelength calibration is applied.

Checks of the spectral calibration in-flight have shown that SCIAMACHY is spectrally very stable. An analysis of on-ground and in-flight (Ahlers, 2004a) data show an absolute shift of the wavelength calibration between  $-0.04$  nm in channel 1 to  $-0.01$  nm in channel 3 and the largest shift

of 0.07 nm in channel 5. The other channels show no significant shift. The reason for the large shift in channel 5 is unknown. However, since the wavelength calibration is calculated from in-flight data and uses the on-ground data only as an initial starting point the shift will not influence trace gas retrievals. More important is the spectral stability of the instrument. Investigations done after launch by Ahlers (2004a) show that the spectral stability is better than the requirement of 0.02 pixels/orbit. Possible exceptions are spectral regions near the channel borders, here a detailed investigation still has to be performed. The blocking shift was also verified in-flight by comparing spectral lines positions from the sun-over-diffuser measurements to those of SLS measurements (Ahlers, 2004b). The difference between the wavelength calibration derived from SLS measurements (not applying the blocking shift correction) and sun measurements is up to 0.15 nm, suggesting an increase of the blocking shift. However, the sun measurements show a large spread and the fit used to determine the wavelengths has a lower accuracy. Therefore, it is not clear if the blocking shift has increased or if this is only an artifact caused by the lower quality of the fit of the sun measurements. Further investigations are needed for clarification.

## 6 Stray light

There are two types of stray light ( $S_{\text{stray}}$  in Eq. 1), *spectral* stray light and *spatial* stray light. Spectral stray light is light of a certain wavelength that is scattered to a detector pixel 'belonging' to a different wavelength. It can lead to distortions of the shape of the spectrum. The reason is usually a reflection in the instrument after the dispersion of the light beam. Spectral stray light can originate from the same channel (intra-channel stray light) or it can scale with the intensity in a different channel (inter-channel stray light). Spatial stray light enters the telescope from outside the IFoV. Spatial stray light is dispersed in an identical way as the light from the observation target. Depending on the source of the stray light it can add an additional offset to the spectrum and/or can distort the spectrum if the primary source of the stray light has spectral characteristics that differ significantly from the observed target. Stray light is usually characterised as a fraction of the total measured intensity for a given pixel.

### 6.1 Spectral stray light

Ideally, in the spectral stray light determination the stray light contribution from each individual pixel to all other pixels would be measured separately. However, this so-called full matrix approach is not always feasible. In the case of SCIAMACHY a  $8192 \times 8192$  matrix would be required making the calculation of stray light very slow. Another problem is that usually only a very small fraction of the incoming light is stray light. If the full matrix approach is used, the signal in

one pixel does only produce a very weak stray light signal in the other pixels which can very well be below the measurement threshold. In order to avoid the problems related to the full matrix approach the spectral stray light for SCIAMACHY was separated into three types: (1) Uniform stray light, (2) ghost stray light and (3) channel 1 stray light. Each type of stray light was characterised on-ground using measurements employing a monochromator. A monochromator gives light in a narrow, well-defined spectral band. The central wavelength of the spectral band can be adjusted. In the derivation of the stray light fractions from monochromator measurements it is assumed that any signal in detector pixels outside this spectral band is caused by stray light. During the on-ground calibration the spectral stray light was measured by changing the central wavelength of the monochromator spectral band, covering the whole wavelength range of SCIAMACHY. The integrated light of the monochromator peak(s) is divided by the light detected outside the peak, giving the stray light fraction. The resulting data are part of the calibration data set and are used to correct the spectral stray light in flight.

The first type of spectral stray light, the uniform stray light, is caused by a diffuse reflection that adds signal to all detector pixels in a given channel. It is by definition not dependent on wavelength. The uniform stray light fraction is calculated in channels 2–8 relative to the average signal in the channel and has values between 0.07% and 0.1% depending on the channel. The relative error of the uniform stray light value from the on-ground calibration is between 15% and 40% of the calculated value, again depending on the channel. Even if the maximum error is assumed, the largest expected stray light fraction is 0.14% which is well within the requirements. It is assumed that the uniform stray light is not dependent on polarisation.

Ghost stray light is caused by a more or less focused reflection of one part of a spectrum to another part of the spectrum. It can distort the shape of the "true" spectrum, because it does not add signal to all pixels equally. The effect of the ghosts on the retrieval depend very much on the shape and dynamic range of the measured spectrum and are not easily predictable. During the on-ground measurements 15 ghost signals were detected in channels 2–8. The total sum of ghost stray light in a channel is at maximum 1% of the incoming intensity. The current correction does not consider the polarisation of the light, an investigation if the polarisation has to be taken into account is planned for the future.

For channel 1 the situation is less favourable with respect to stray light levels. The on-ground measurements showed that the spectral stray light in channel 1 can be up to 10% of the incoming signal for a typical input spectrum. It is also highly wavelength dependent. The main reason for the larger stray light fraction in channel 1 is the high dynamic range of the spectra in this channel, with the lowest signal 3 orders of magnitude smaller than the highest signal. The coarse, artificial separation in uniform and ghost stray light

is not sufficient for a correction in channel 1 and an alternative method had to be formulated. The chosen approach combines the correction of uniform and ghost stray light in a modified matrix approach. In order to avoid signal-to-noise problems during the spectral stray light measurements, 10 wavelengths bands were defined separately for s and p-polarised light leading to a total of 20 bands. For both polarisation directions 9 bands were located in channel 1 to characterise intra-channel stray light and 1 band covered the signal from channels 2–5 to characterise inter-channel stray light.<sup>3</sup> For each band the stray light contribution to all detector pixels was calculated leading to a  $10 \times 1024$  matrix for both, s- and p-polarised light. The correction has an accuracy of around 25% and reduces the stray light by an order of magnitude leaving at most 1% stray light in the spectrum after correction.

## 6.2 Spatial stray light

Spatial stray light is clearly observed in SCIAMACHY limb measurements at altitudes above 90 km and in data taken in Nadir configuration over the North pole. The latter is expected since at that position in the orbit the sun shines directly into the limb port of the instrument producing a considerable amount of stray light. In order to minimise stray light above the Pole the ASM is rotated such that the edge of the diffuser/mirror points in flight direction preventing a direct reflection into the telescope. The observed stray light in this orbit position is caused by remaining reflections of sun light from the baffles and other parts of the Limb port. The stray light in Limb measurements was not expected and was first discovered in measurements taken at 150 km tangent height, where no atmospheric light should be present. These measurements were originally intended to determine the orbital variation of the dark signal in channel 8 (see Sect. 4.2) and as an optional dark correction for the Limb measurements. Investigations (van Soest, 2005) show that the stray light is not caused by a light leak, because spectral structures like air glow emissions and atmospheric absorptions are visible in the measurements, which means that the signal is spectrally dispersed and thus goes through the optics of the instrument. Comparison with MERIS data showed that the stray light does not correlate with the intensity of the scene at the sub-satellite point, ruling out the possibility that light is entering through the Nadir port and is subsequently directed into the telescope. Measurements of the Limb scans at high altitude and Limb scans at a lower tangent altitude of 10 km show a good correlation confirming that the stray light is caused by light entering the instrument through the slit from regions outside the IFoV. The stray light is highest in channel 2–4 and is very low in channels 1, 5 and 6. The effect of the stray

<sup>3</sup>The channel 1 detector material is not sensitive for light with wavelengths above 1000 nm, so the IR channels do not have to be considered.

light on the Limb retrievals will be assessed in a future investigation. The Limb scan has been adjusted to take the dark measurement at 250 km instead of 150 km on 26 May 2003 (orbit 6456). At that height the spatial stray light is reduced by an order magnitude to 5–10 BU/s making an estimation of the orbital variation of the dark signal possible. However, the dark signal correction of the data should be done with the dark signal derived from eclipse data.

## 7 Polarisation

### 7.1 Theoretical concept

SCIAMACHY is – as all grating spectrometers without a polarisation scrambler – sensitive to the polarisation of the incoming light, i.e. the response will not only depend on the intensity but also on the polarisation of the light. In the polarisation correction the instrument is represented by a so-called Mueller matrix and the light is represented by the Stokes vector (see e.g. Coulson, 1988):

$$\begin{pmatrix} S \\ Q \\ U \end{pmatrix}_{\text{det}} = \begin{pmatrix} M_{11} & M_{12} & M_{13} \\ M_{21} & M_{22} & M_{23} \\ M_{31} & M_{32} & M_{33} \end{pmatrix}^{D,P} \begin{pmatrix} I \\ Q \\ U \end{pmatrix}_0 \quad (4)$$

On the left hand side of the equation we have the light as detected by the instrument, i.e. in front of the detectors. On the right hand side we have the Mueller matrix  $\mathbf{M}_{\text{inst}}$  describing the response of the instrument ( $D$  denotes the science channels,  $P$  the PMD channels) to the incoming light represented by the Stokes vector. The first element of the Stokes vector,  $I$ , denotes the total intensity of the light (we use  $S$  for the detected signal here).  $Q$  is a measure for the polarisation along the x or y-axis of a chosen reference frame and can be described as  $Q = I_x - I_y$ .  $U$  is a measure for the polarisation along the  $\pm 45^\circ$  direction and is defined as  $U = I_{45} - I_{-45}$ . Note that the total intensity can be written as  $I = I_x + I_y$  or as  $I = I_{45} + I_{-45}$ . Often  $Q$  and  $U$  are normalised to the total intensity  $I$ , we will denote normalised fractions with  $q$  and  $u$  in the remainder of this paper. Note that the formula above is only correct for Earth observations where the circular polarisation of the light  $V$  can be neglected. This is usually the case (see e.g. Hansen and Travis, 1974) and thus circular polarisation is not considered in the polarisation correction. All Mueller matrix elements are dependent on wavelength and on the incidence angle of the light on the scan mirror(s) or diffuser. In the calibration, ambient measurements on component level and instrument T/V measurements have to be combined meaning that the actual instrument matrix has to be calculated by a multiplication of the matrix for the scanner (combination) and the OBM. However, we will not go into detail in this paper and will just use  $\mathbf{M}_{\text{inst}}$  as the instrument matrix describing the complete instrument. Note that each observation mode has its own matrix, e.g. the Mueller matrix for Nadir observations is not the same as the matrix

for Limb observations. For more information, the reader is directed to Slijkhuis (2000) and Frerick (1999). The Stokes parameters relate in the following way to the polarisation angle  $\chi$  and the degree of linear polarisation  $P$ :

$$\chi = \frac{1}{2} \arctan\left(\frac{U}{Q}\right) \quad (5)$$

$$P = \sqrt{Q^2 + U^2}/I \quad (6)$$

The detectors of SCIAMACHY are only sensitive to the intensity reducing Eq. (4) to

$$S_{\text{det}} = M_{11}^D \cdot I \cdot \left(1 + \frac{M_{12}^D}{M_{11}^D} \cdot q + \frac{M_{13}^D}{M_{11}^D} \cdot u\right) \quad (7)$$

where  $I$  is the intensity and  $q$  and  $u$  the polarisation fraction of the incoming light, and  $S_{\text{det}}$  is the detected intensity.  $M_{11}^D$  is the radiometric response function of the science detectors (see Sect. 8) and the reciprocal of the term in brackets is in effect the desired polarisation correction factor. Note that we are leaving out here the so-called m-factors that take into account a possible degradation of the light path (see Sect. 9.3). The m-factors correct for each light path long term degradation of the instrument. For details the reader is referred to Slijkhuis (2000).

## 7.2 Calculation of the polarisation correction

The calculation of the polarisation correction is the most complicated part of the calibration of SCIAMACHY data. Therefore we will first describe the general steps that have to be done and after that go into some more detail. The basic steps are

1. Definition of polarisation reference frames to be able to convert calibration data to the correct observation reference frame.
2. Determination of the polarisation sensitivity of the instrument:
  - (a) Measurement of the instrument response to polarised light which is stored as calibration data
  - (b) Translation of the calibration data into the Mueller matrix approach
3. Calculation of the polarisation of the incoming atmospheric light
  - (a) Determination of  $Q$  and  $U$  for single scattering in the UV
  - (b) Determination of  $Q$  and  $U$  from PMD D and PMD 45, these two measure the polarisation for the same wavelength range (but see also Sect. 7.3)
  - (c) Determination of  $U$  and  $Q$  for the PMD A–C, E, F wavelengths using a theoretical  $U/Q$  ratio
4. Interpolate the  $Q$  and  $U$  values to the full wavelength grid of SCIAMACHY

### 7.2.1 Polarisation reference frames

Two reference frames are used for SCIAMACHY: the *calibration reference frame* used for calibration measurements and the *observation reference frame* used in the data product. The polarisation reference frame used in the calibration is defined w.r.t. the direction of the slit: looking in the direction of the light entering the instrument after the scan mirrors, the  $+45^\circ$  polarisation direction is obtained by a  $45^\circ$  clockwise rotation from the p-polarisation direction. The p-polarisation direction is aligned with the long side of the entrance slit of SCIAMACHY. The polarisation reference plane used for measurement data is the local meridian plane containing the satellite, the zenith and the centre of the FOV with the flight direction pointing into the negative y-direction and the z-direction pointing to the instrument. In this reference frame the p-polarisation ( $q=-1$ ) is parallel to the plane and the  $45^\circ$  direction can be obtained by rotating counter-clockwise from the +x-direction to the +y-direction. This reference frame differs from that used in the calibration making a coordinate transformation necessary. The data processor handles all transformations from the calibration reference frame to the observation frame and v.v. internally. The calculated polarisation fractions in the Level 1 data product are those in the *observation* polarisation frame.

### 7.2.2 Determination of the instrument polarisation sensitivity

The polarisation sensitivity was measured on-ground using ratios of measurements as far as possible to minimise influences of the measurement set-up on the data. SCIAMACHY shows a different sensitivity to s- and p-polarised light and to  $+45^\circ$  and  $-45^\circ$  polarised light<sup>4</sup>. In order to correct the measurements of the atmosphere, the following quantities have to be measured: (1) The sensitivity to s-polarised light relative to p-polarised light. This is called  $\eta$  and is derived from ratios of measurements with fully s- and fully p-polarised light. (2) The sensitivity of  $+45^\circ$  polarised light to  $-45^\circ$  polarised light. This quantity is called  $\zeta$  and is determined from ratios of measurements using  $+45^\circ$  and  $-45^\circ$  polarised light. (3) To be able to determine the atmospheric polarisation, also the ratio of the signals in the PMDs to the signal in the science detectors was determined for all four polarisation directions. Care was taken to ensure that the intensity in all these measurements was the same, because otherwise a difference in intensity could have been mistaken for an effect of the polarisation of the light. The Mueller matrix elements from Eq. (7) relate in the following way to  $\eta$  and  $\zeta$ :

$$\frac{M_{12}^D}{M_{11}^D} = \frac{1 - \eta}{1 + \eta} \quad (8)$$

<sup>4</sup>The latter is a consequence of a rotation of the polarisation direction of the incoming light by the pre-disperser prism, due to stress induced birefringence in the prism.

$$\frac{M_{13}^D}{M_{11}^D} = \frac{1 - \zeta}{1 + \zeta} \quad (9)$$

Using Eq. (7) we can define  $c_{\text{pol}}$  from

$$I = c_{\text{pol}} \cdot \frac{S_{\text{det}}}{M_{11}^D} \quad (10)$$

Combining the above equation with Eqs. (8) and (9) the polarisation correction factor  $c_{\text{pol}}$  written in terms of the on-ground measurements is

$$c_{\text{pol}} = \left[ 1 + \frac{1 - \eta}{1 + \eta} \cdot q + \frac{1 - \zeta}{1 + \zeta} \cdot u \right]^{-1} \quad (11)$$

with  $q$  and  $u$  being the polarisation fractions of the incoming light, which have to be determined in the following steps. Note that  $c_{\text{pol}}$  depends on wavelength, on the scan angle of the mirror(s) and the observation mode, i.e.  $c_{\text{pol}}$  is different for Nadir and Limb observations.

### 7.2.3 Calculation of the polarisation of the atmospheric light

For the determination of  $q$  and  $u$ , the on-board PMDs and theoretical models are used. Only a short summary of the polarisation calculation is given here, for details the reader is referred to Slijkhuis (2000). First the polarisation is determined for a few individual points. The polarisation near 300 nm (where no PMD is measuring) is determined theoretically from the scattering geometry in a single scattering approximation. The ratio of the signal in the science detectors and the PMDs is used to determine the polarisation for the central wavelengths of the PMDs. Since the PMDs have a much wider bandwidth than the science detectors, mathematically the signal  $S_{\text{PMD}}$  in the PMDs is written as the sum over a number of “virtual pixels” that have the same characteristics as the corresponding science channel pixels. This gives the following equation for the signal  $S_{\text{PMD}}$

$$S_{\text{PMD}} = \sum_{i=\lambda_{\text{start}}}^{\lambda_{\text{end}}} M_{11}^{P,i} I_{0,i} \cdot \left( 1 + \frac{M_{12}^{P,i}}{M_{11}^{P,i}} \cdot q + \frac{M_{13}^{P,i}}{M_{11}^{P,i}} \cdot u \right) \quad (12)$$

with  $M_{xx}^{P,i}$  being the Mueller matrix elements as derived from the on-ground PMD calibration for the virtual pixel  $i$  covering a certain wavelength and  $\lambda_{\text{start, end}}$  denoting the wavelength range of the PMD. Note that the PMDs A-F show a weak sensitivity to  $u$  and that the signal of PMD 45 is weakly dependent on  $q$ . Therefore, additional assumptions have to be made to determine  $q$  and  $u$  from the PMDs. First the polarisation fractions are determined iteratively from PMD D and PMD 45 (these 2 PMDs measure  $q$  and  $u$  at the same wavelengths)<sup>5</sup>. Then  $q$  and  $u$  are determined using the following assumptions for  $u/q$ :

<sup>5</sup>Note that in the current processor version 5.04 the  $u$  value is derived from a theoretical  $u/q$  using the measured  $q$  value from PMD D instead of the described approach, see Sect. 7.3.

- The value of  $u/q$  for wavelengths smaller than a pre-defined wavelength  $\lambda_{\text{single}}^{\text{sc}}$  is set to the single scattering value assuming that in this wavelength range single scattering dominates.
- For wavelengths larger than a wavelength  $\lambda_{\text{Aerosol}}$  the value of  $u/q$  is set to the value determined from PMD D and PMD 45 assuming that in this spectral region aerosol scattering and clouds dominate the polarisation of the light.
- In between  $\lambda_{\text{single}}^{\text{sc}}$  and  $\lambda_{\text{Aerosol}}$  a linear interpolation to the central wavelengths of the PMDs is used.

It is also possible to use the channel overlaps to determine the polarisation. The wavelength range of all channels except channels 6 and 7 and channel 7 and 8 overlap (see Table 1). In the overlap regions the same signal is measured, but the polarisation sensitivity is different in the two overlapping channels. One can exploit this difference to determine the polarisation. However, so far  $q$  and  $u$  values determined from the overlaps are not very realistic. This is possibly related to problems with the low signal in the science channels near the channel boundary and problems with the radiometric calibration in that region (see e.g. Tilstra and Stammes, 2004). In the current data processor version 5.04 the channel overlaps are not used to determine  $c_{\text{pol}}$ .

### 7.2.4 Interpolation to full wavelength grid

The result of the calculations described above are 7 values for  $q$  and  $u$ , 6 values at the central wavelengths of the PMDs and one single scattering value at 300 nm. The final step in the polarisation algorithm is an interpolation of  $Q$  and  $U$  to the full wavelength grid of the science channels. The polarisation fractions for wavelengths between the wavelengths of PMD A and PMD F are calculated by an Akima interpolation (Akima, 1970), the polarisation fractions below 300 nm are set to the single scattering value and the fraction for wavelengths beyond the PMD F wavelength are set to the PMD F value. That leaves the region between 300 and 340 nm. The polarisation degree in this region changes rapidly due to the strong decrease of O<sub>3</sub> absorption. No PMD measurements are available here. In order to obtain the polarisation fractions in this region the so-called Generalised Distribution Function (GDF) which was originally developed for GOME (Aberle et al., 2000) is used. The connection between the wavelength regions where different methods are used is done such that the gradient of the resulting curve remains continuous.

The polarisation correction factor  $c_{\text{pol}}$  can now be calculated for the whole wavelength range using  $q$ ,  $u$  and  $\eta$ ,  $\zeta$  in Eq. (11).

### 7.3 Problems

Looking at Eq. (11) one limitation of the calibration approach becomes clear. The polarisation correction is dependent on the accuracy of the  $q$  and  $u$  determination. The polarisation sensitivity (see Fig. 3) shows spectral features especially in channels 1–3 and in the channel overlaps. Whenever there is an error in the determined polarisation fractions, these spectral features will be visible in the *polarisation corrected* spectra. The measurement of the polarisation in SCIAMACHY with broadband sensors inevitably introduces an – unknown – error into the polarisation fractions. The spectral features in the polarisation sensitivity will be re-introduced through the polarisation correction, scaled by the error in  $q$  and  $u$ . A preliminary investigation showed that this is mostly an issue for channels 1–5, where the atmospheric polarisation is relatively high. Since the instrument is more sensitive to the  $q$  polarisation fraction, a large error here affects the spectra the most while an error in the  $u$  fraction is negligible in most cases. For retrievals large features and features that correlate with a spectral structure of trace gases are most critical, a slow variation over the channel is less critical. Channel 1 and 2 show a strong sensitivity and are most susceptible to errors in the polarisation fractions (for an example see Tilstra and Stammes, 2005). A spectral feature of  $\eta$  and  $\zeta$  around 480 nm in channel 3 prohibits DOAS retrievals of  $O_3$  in that spectral window. Further investigations are planned.

However, not all problems are necessarily related to an error in the determination of the polarisation fraction. Experience has shown that in the past errors in the data processor, in the derivation of the polarisation sensitivities from on-ground measurements and in the conversion of the different polarisation reference frames led to an incorrect polarisation correction. The processor and the calibration data were reviewed by SRON, DLR, TPD and IfE and both were corrected where necessary. Still, there are a few remaining problems. A check of the derived polarisation fractions shows that the values derived from PMD A for limb configurations are still unphysical for some observation geometries (see Fig. 4, bottom). In addition, with the current calibration data and processor version 5.04 it is not possible to derive correct  $u$  values (see Fig. 4, top). The reason is still not clear, but possible causes are stray light in PMD 45, systematic errors during the on-ground calibration or a problem with the data processor algorithm. In view of the problems, it was decided not to use the original approach as it is described in the previous section to determine  $u$ . Schutgens et al. (2004) show that an approach based on the single scatter value of the polarisation leads to good results for most observation geometries and ground scenes. Therefore, the current version of the data processor determines  $u/q$  from a single scattering approach for the whole wavelength range to calculate a  $u_{\text{single}}/q$  until the reason for the unphysical  $u$  values determined from PMD 45 and PMD D is found. Investigations for a solution are ongoing.

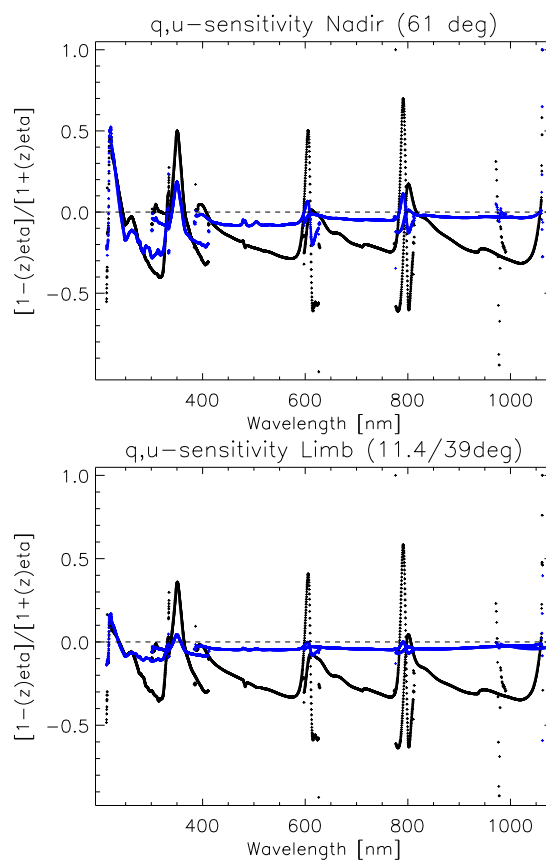


**Fig. 3.**  $q$  (black) and  $u$  (blue) sensitivity from Eq. (11) for Nadir,  $61^\circ$  elevation angle (top) and Limb,  $11.4^\circ/39^\circ$  elevation/azimuth angle (bottom) for channels 1–5. Note that these sensitivities are multiplied with the polarisation fractions to get  $c_{\text{pol}}$  and the correction values will thus be smaller for lower polarisation.

The polarisation correction in the IR (PMD F) suffers from the transmission loss due to ice in channels 7 and 8 (see Sect. 9.1), since the polarisation fractions are determined using the ratio between the signal in the science channels and the PMDs. A correct retrieval requires a correction of the transmission in the IR channels. This is not yet implemented in the data processor. Other – most likely minor – effects that possibly change the polarisation sensitivity in the IR channels are the detector temperature change and the ice layer itself. Here, a study still has to be performed. It is recommended not to use the polarisation correction in the IR until at least the transmission correction is implemented. Since the polarisation in that wavelength range is relatively weak, the impact of not correcting for the polarisation sensitivity of the instrument is expected to be moderate.

In Limb observations, the calculated polarisation showed an unexpected drift with increasing tangent height. This is maybe related to the spatial stray light in Limb observations (see Sect. 6.2). Therefore, a scaling factor is applied to the polarisation measured at 30 km to calculate the polarisation

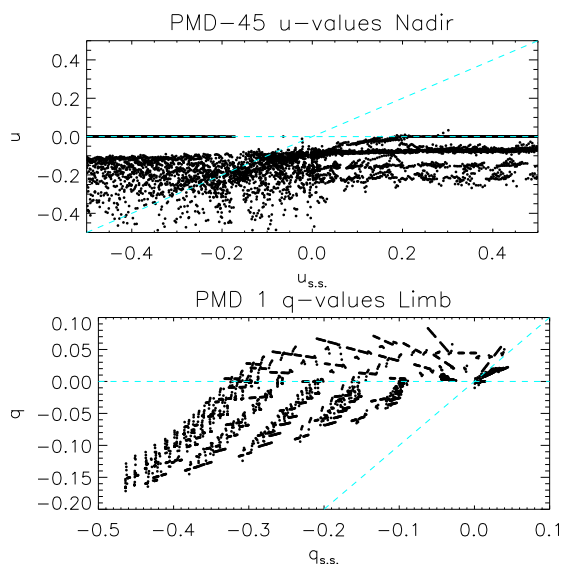


**Fig. 4.** Top:  $u$  values as derived in the processing of PMD 45 and PMD D data for orbit 15975 (21 March 2005). Bottom:  $q$  values derived from PMD A (UV, channel 2 wavelength region). Shown is the derived value (y-axis) against the theoretical, single scattering value. The dashed lines mark the unpolarised case and the single scattering case. All derived polarisation fractions outside the dashed lines are not in the allowed, physical range. Note that the data were filtered for rainbows and sun glint, so unphysical values are not caused by these effects.

at larger tangent heights. This is allowed, because the depolarisation remains constant above this height (McLinden et al., 2002).

An additional problem in the polarisation correction algorithm is related to the cluster concept (Tilstra et al., 2005). Jumps in the reflectance spectrum can appear between clusters with different integration times after normalization to the integration time. The polarisation correction at shorter integration times is generally not as good as for longer integration times, because information from the missing parts of the spectrum in the channel is needed for a successful correction. This information has to be approximated for short integrations, since data from clusters with a longer integration time are not available in every readout (see last paragraph of Sect. 2). This can lead to an erroneous polarisation correction causing jumps at cluster boundaries.

In the meantime, alternative polarisation correction methods for the UV have been proposed by Tilstra and Stammes (2005) and Hasekamp et al. (2002). These methods incorporate the polarisation sensitivities  $\eta$  and  $\zeta$  themselves to determine a correction for the polarisation.

## 8 Radiometric calibration

### 8.1 Concept and on-ground measurements

The final step in the calibration of the data is the radiometric calibration. The retrieval of trace gases usually uses the reflectance, the ratio of the radiance reflected from the Earth's atmosphere and solar irradiance. The solar irradiance is measured with on-board diffusers in-flight. Using Eqs. (7) and (11) the reflectance can be written as

$$R = \frac{\pi \cdot I_{\text{Earth}}}{\mu_0 \cdot I_{\odot}} = \pi \cdot \frac{S_{\text{det}}^{\text{Earth}} \cdot c_{\text{pol}}}{\mu_0 \cdot M_{11}^{N,L}} \cdot \frac{M_{11}^{\odot}}{S_{\text{det}}^{\odot}} \quad (13)$$

with  $I_{\text{Earth},\odot}$  and  $S_{\text{det}}^{\text{Earth},\odot}$  as the Earth and sun intensity and measured signal,  $\mu_0$  the cosine of the solar zenith angle, and  $M_{11}^{\odot}$  the radiometric responses for sun-diffuser measurements.  $M_{11}^N$  is the radiometric response for nadir and has to be used for nadir measurements, while  $M_{11}^L$  has to be used for limb measurements. For a proper calibration the instrument responses have to be determined as a function of wavelength  $\lambda$  and incidence angle  $\alpha$ . As already mentioned in Sect. 3 the radiometric response was measured on instrument level under T/V conditions and the mirror (combination) and the mirror diffuser combination were measured under ambient conditions. In order to transfer ambient measurements to T/V measurements the ratio of a T/V measurement to an ambient measurement at the same incidence angle, the reference angle  $\alpha_0$  is used:

$$C_A(\lambda, \alpha_0) = \frac{\mathcal{R}(\lambda)}{\eta_{\text{OBM}}(\lambda) \cdot R_s^N(\lambda, \alpha_0) + R_p^N(\lambda, \alpha_0)} \quad (14)$$

where  $\mathcal{R}$  is the radiometric response measured under T/V conditions in nadir configuration,  $\eta_{\text{OBM}}$  is the polarisation sensitivity of the OBM without the scan mirrors and  $R_{s,p}^N$  is the reflectivity of the nadir mirror for s- and p-polarised light. Using this relation, the radiometric response for Earth observations and sun observations can be written down as

$$M_{11}^{N,L}(\alpha) = C_A \cdot [\eta_{\text{OBM}} \cdot R_s^{N,L}(\alpha) + R_p^{N,L}(\alpha)] \quad (15)$$

$$M_{11}^{\odot}(\alpha) = C_{\text{NDF}} \cdot C_A \cdot [\eta_{\text{OBM}} \cdot \eta_{\text{NDF}} \cdot B_s(\alpha) + B_p(\alpha)] \quad (16)$$

where  $\alpha$  is the incidence angle on the mirror and diffuser,  $C_{\text{NDF}}$  is a factor that corrects for the Neutral Density Filter (NDF) that is in the light path for sun measurements,  $\eta_{\text{NDF}}$  is the polarisation sensitivity of the NDF and  $B_{s,p}$  is the reflectivity of the combination ASM mirror + ESM diffuser. Note that all elements of the above equations are wavelength dependent. The term in brackets in the above equations constitutes the so-called scan angle correction, which is derived from ambient measurements. The reflectance in terms of calibration measurements and detector signal becomes (using the above two equations and Eq. 13)

$$R = \pi \cdot \frac{c_{\text{pol}} \cdot S_{\text{det}}^{\text{Earth}}}{\mu_0 \cdot S_{\text{det}}^{\odot}} \cdot \frac{C_{\text{NDF}} \cdot [\eta_{\text{OBM}} \cdot \eta_{\text{NDF}} \cdot B_s(\alpha_1) + B_p(\alpha_1)]}{[\eta_{\text{OBM}} \cdot R_s^{N,L}(\alpha_2) + R_p^{N,L}(\alpha_2)]} \quad (17)$$

It was already mentioned that SCIAMACHY can measure the solar spectrum in two ways: Using the ESM diffuser (this is the originally foreseen way) and using the ASM diffuser. The ESM diffuser showed large spectral features of 1–3% in on-ground measurements. Model calculation predicted that the retrieval of many products (e.g. BrO, SO<sub>2</sub> or OCIO) with DOAS could be made impossible by the spectral features (de Beek, R., Bovensmann, H., 2000). An analysis of in-flight data was done by Ahlers et al. (2004) and confirmed the presence of spectral features. The ASM-diffuser has been installed in a later stage on the back side of the mirror, after investigations of on-ground measurements revealed the presence of the spectral features. This diffuser is manufactured differently from the ESM diffuser leading to much smaller spectral features. No absolute calibration of the ASM diffuser could be performed, because SCIAMACHY was already integrated with ENVISAT when the diffuser was installed. Preliminary investigations showed that DOAS retrievals are significantly improved by using data of the ASM diffuser for the solar reference (see e.g. Sierk, 2003). Therefore, for DOAS retrievals that have an insufficient quality using the ESM diffuser spectrum, the usage of the ASM diffuser solar reference should be considered. After the update of the data processor to version 6.0, both solar references will be available in the Level 1 product.

## 8.2 Problems

Shortly after launch comparisons of modelled sun spectra from Kurucz (1995) and measured sun spectra showed that the solar irradiance measured with SCIAMACHY was around 10 % too high for all wavelengths (see e.g. Skupin et al., 2003; Gurlit et al., 2005). The reflectance on the other hand was around 10–20% too low as comparisons with GOME (Tilstra et al., 2003; Latter et al., 2003), MERIS (Acarreta and Stammes, 2005) and radiative transfer models (van Soest et al., 2005) revealed. The deviations could be traced back to two causes: (1) a wrong absolute value of the reflectivity  $B_{s,p}$  (see Eq. 16) and (2) a insufficient scan angle correction derived from the ambient measurements. In the daily solar irradiance measurements in-flight 30 individual spectra of the sun are taken. During these measurement the incidence angles on the diffuser change due to the movement of the satellite relative to the sun. The insufficient angle correction was identified with the help of an additional set of on-ground calibration measurements with the same incidence angles as in the first in-flight ESM diffuser sun measurement. The data were not used for the radiometric calibration, since the instrument had to be tilted in the vacuum tank for these measurements making measurements in nadir configuration impossible. The sun irradiance derived from these data came close to known standards (Ahlers, 2003). The on-ground data used for the radiometric calibration were measured with a different geometry not matching the in-flight incidence angles and was relying on the scan angle correction

from ambient data.

The reason for the inadequate scan angle correction and the wrong absolute value of  $B_{s,p}$  is unclear. It could be either an error in the algorithms that were used to calculate  $B_{s,p}$  from the ambient measurements or not all effects of the measurements set-up were taken into account. It is conceivable that the illumination conditions during the measurements made for  $B_{s,p}$  were different from those encountered in-flight or that detector effects were not fully corrected (the ambient measurements were done on component level, not using the instrument detectors). SRON will review the on-ground calibration and the used algorithms to find possible errors. However, a complete review will take some time and although DOAS type retrievals do not rely on the absolute values of the reflectance, the retrieval of the aerosol optical thickness, cloud fraction algorithms, the determination of the surface albedo and vertical ozone profiles from nadir need radiometrically accurate data. Without a proper correction to the radiometric calibration these products loose accuracy.

In order to provide useful data before the review is finished, a new radiometric calibration data set was calculated by IfE (Noël, 2005) with input from SRON and TPD. TPD provided a new scan angle correction for  $B_{s,p}$  (Schrijvers, 2004) and the raw, on-ground measurement data, SRON provided the new non-linearity (Kleipool, 2003) and memory effect correction (Lichtenberg, 2003) and an in-flight derived NDF transmission. IfE calculated from these inputs new calibration data, improving the interpolation of the ambient data to the full grid, correcting an apparent error in the ambient characterisation of the limb reflectivity  $R_{s,p}^L$  and incorporating a new absolute value for the reflectivity  $B_{s,p}$ . Two different calibration data sets were calculated in this way, using two different types of on-ground data, the “spectralon” data measured with a NIST calibrated FEL lamp and the “NASA sphere” data measured with an internally illuminated, BaSO<sub>4</sub> coated sphere already used in NASA’s SBUV and TOMS programs for absolute radiometric calibration. Both calibration data sets were tested by KNMI in September 2004 using a set of 3 reference orbits.

The result of these tests were

- both new calibration data sets improve the offset value of the reflectance, the comparison with MERIS and Doubling-Adding KNMI (DAK) radiative transfer model show a deviation of at maximum 5%,
- the new calibration data introduce spectral features, most dominant around 350 nm (not polarisation related) and 880 nm,
- the spectralon data show better results than the NASA sphere data.

On the basis of these results the new spectralon calibration data will be implemented in the data processing update. Further verification and validation will be performed to assess

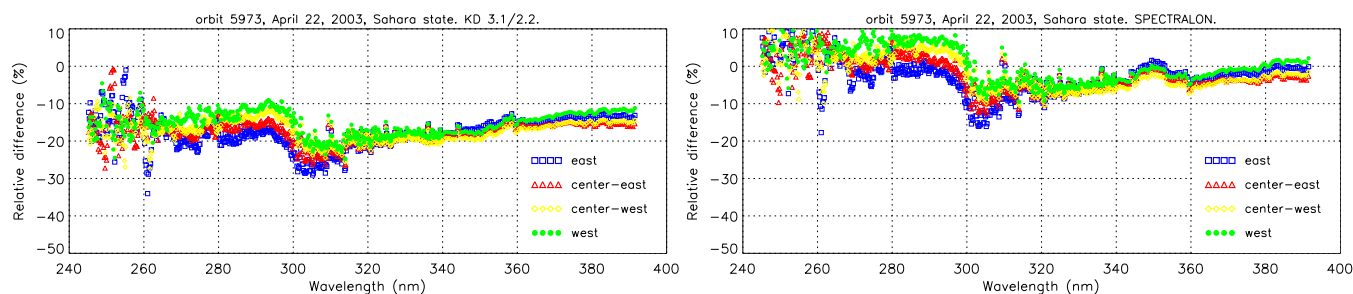


**Fig. 5.** Comparison of SCIAMACHY calculated reflectance with model calculations, using original calibration data (left) and “spectralon” calibration data (right). It can clearly be seen that the new radiometric calibration improves the overall offset of the reflectance, but also introduces a new spectral feature around 350 nm. Note that the dip around 300 nm is probably an artifact caused by insufficient characterisation of the ozone profile in the model (figure taken from Tilstra et al., 2004).

the quality of the new calibration and to assess the impact of the spectral features that were introduced.

## 9 In-flight effects

### 9.1 Ice in channels 7 & 8

Shortly after the very first cooling of the detectors, a significant loss of transmission in channel 7 and 8 was discovered. Investigations showed that an ice layer growing on top of the cylindrical lens covering the detectors was responsible. Only channel 7 and 8 are affected because these channels are cooled down to around 145 K while the other channels have temperatures of 200 K or higher (see Table 1). A likely source of the contamination is the carbon fibre supporting structure of ENVISAT itself, since it is known that carbon fibres can accumulate a substantial amount of water. The water contained in the fibres started to gas out once the satellite was in orbit. SCIAMACHY is covered by a double layer of multilayer insulation (MLI) blankets, one from ENVISAT and one from the instrument itself to prevent strong thermal gradients while in orbit. The MLI has a number of venting holes to allow the outgassing of the instrument and prevent a contamination of surfaces, but apparently the venting volume allowed by the holes is not large enough or the holes are obstructed. Thus, the contaminant is not (or too slowly) removed from the instrument volume. Other instruments on ENVISAT have also reported problems due to contamination (see e.g. Perron, 2004; Smith, 2002).

Under the assumption that the ice layer consists purely of water ice the layer thicknesses can be calculated using an absorption coefficient from Grundy and Schmitt (1998). The ice layer thickness is up to  $230\ \mu\text{m}$  ( $600\ \mu\text{m}$ ) in channel 7 (channel 8) six months after a decontamination. In order to remove the ice from the detectors and to restore the transmission, regular decontaminations at high temperatures are performed. The only heater on-board having enough power to heat the detectors to sufficiently high temperatures is the decontamination heater of the SRC which was installed to

clean the SRC when the amount of contaminants on its surface starts to decrease its cooling power. The drawback of using this heater is that it is not possible to heat channels 7 and 8 separately from the other channels, the heating always raises the temperatures of all channels leading to a substantial loss of data quality during decontamination periods. In order to properly remove all the ice from the detectors and their immediate vicinity, a decontamination period of 300–370 h has been found to be most effective. During a decontamination the detector temperatures are raised to about 280 K. The OBM is also heated to around 265 K to prevent ice settling on OBM elements. After each decontamination the transmission is fully restored. The growth of the ice layer in channel 8 is shown in Fig. 6. The calculation of the layer thickness was done for spectral bins of 64 detector pixels with the appropriate absorption for each wavelength bin. In both channels the ice layer is thicker at the beginning of the channel (the blue end) than at the end of the channel at higher wavelengths. The reason for this is unclear. The thermal coupling from the detector to the cooler is positioned in the centre of the channel, so one would expect the ice layer to be thickest in the middle of the channel if the thermal gradients over the detector array were strong enough.

The long term development of the transmission in both channels is very different. While channel 8 shows more or less the expected behaviour with an exponential-like decay of the transmission after each decontamination when the ice layer starts to grow again, channel 7 shows erratic behaviour (see Fig. 7). After the decontaminations in August 2003 (black x’s) and June 2004 (blue triangles) the transmission declined very rapidly and linearly reaching a minimum after around 20 days. Then the transmission slowly increased. After the decontamination of January 2004 (blue crosses) and 2005 (red diamonds) a completely different behaviour is observed with constant transmission at a very high level. The reason for the erratic behaviour of channel 7 is not known. One hypothesis is that a second cold trap resides somewhere in channel 7. This second cold trap is activated under certain circumstances and collects the majority of water vapour

before it can settle on the detector lens. However, this explanation is purely based on the observed transmission behaviour of channel 7 and up to now no part of the detector module could be identified as a second cold trap. The difference in the behaviour of channel 7 and 8 is puzzling, since both channels are of identical design and operate at almost the same temperature (the difference is around 1 K). Thus, one would expect a similar behaviour.

Regardless of the reason of the ice layer build-up and its behaviour over time, the calibration and the operations of SCIAMACHY have been adjusted to minimise the effect of the ice. The first adjustment were made to the decontamination frequency. Originally it was required to decontaminate the cooler at least every six months to prevent irreparable damage to the cooler. The in-flight experience has shown that the cooling power did not decrease in 3 years of operations. Therefore it was decided to only do a decontamination, when the transmission in channel 7 and 8 drops below a level where a useful retrieval of trace gases is no longer possible. This prevents a situation like in summer 2004, where the transmission in channel 7 was degraded by 60% in the first 40 days after the decontamination. After that period the transmission increased again, but stabilised around 40% only, i.e. at a much lower level than after previous decontaminations (blue triangles in Fig. 7). Apart from this adjustment in operations, the ice layers lead to the following effects that can affect trace gas retrieval (see also GlouDEMANS et al., 2005):

*Signal-to-noise loss due to transmission loss:* When a sun reference from the same day is used, the effect on the value of the reflectance is only minor since the transmission loss cancels in the ratio of Earth and solar spectrum. However, the overall signals are lower, leading to a decreased signal-to-noise-ratio.

*Change of slit function:* The slit function is changed significantly by the scattering effect of the ice layer on the detector. This scattering is dependent on the thickness and the structure of the ice, which is not uniform over the detector array. A correction scheme using known trace gas contents for a certain geolocation as well as the effect on the retrieval if the slit function is not corrected is presented in GlouDEMANS et al. (2005).

*Change of the dark signal:* The dominant part of the dark signal in channel 7 and 8 is the thermal background (see Sect. 4.2). The thermal background is attenuated by the ice just like any other optical signal on the detector, leading to a variation of the dark signal on the timescale of a few orbits. Thus the IR data have been corrected with a dark signal measured as close as possible to the trace gas measurements. This has been implemented in the data processing in 2004 (version 5.01). In addition, the orbital variation of the background in channel 8 will also change with the transmission. It is currently investigated if this affects retrievals in channel 8.

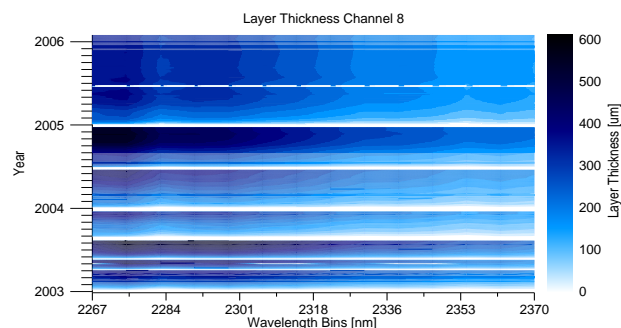


**Fig. 6.** Ice layer thickness over time and as a function of wavelength for channel 8 derived from solar measurements taken between January 2003 and January 2006. The spectrum was divided into 16 wavelength bands (x-axis), each band consisting of 64 detector pixels which corresponds roughly to 8 nm. Only the 14 central bands are shown here. The thickness of the ice layer is indicated by the different colours with darker colours meaning a thicker layer. In the white areas either no data are available or a decontamination is performed. One can clearly see the build up of ice after the decontaminations and that the layer is usually thicker at the short wavelength side of the channel (left side of the plot).

*Change of detector temperature:* The ice also covers the gold plated aluminium structures of the detector suspension. The ice increases the infrared absorption properties and thereby the radiative heating of the detectors. As a result the detector temperature slowly increases. Increase rates directly after a decontamination are around 0.05 K/day going down to 0.02 K/day as the transmission stabilises. The detected signal in channel 8 will change because the quantum efficiency in this channel is dependent on the temperature. However for most purposes this effect is minor compared to the overall effects of the ice and can be corrected for.

## 9.2 Light leak in channel 7

After launch it was discovered that channel 7 shows a spurious signal in Limb dark measurements that is much higher than the spatial stray light found in the other channels (see Sect. 6.2). The signal shows no spectral signature, but is a broadband feature. This excludes the possibility that it is caused by light going through the complete optical system of the instrument. Further investigations were done by SRON to characterise the light leak. In this study, limb dark measurements at 250 km from all available Level 1b data of February 2004 were used to evaluate the light leak of channel 7. In order to determine the magnitude of the light leak, the data were corrected for non-linearity, dark signal (derived from the eclipse part of the orbit) and spectral stray light. Ideally, the signal should be zero after the corrections. Figure 8 shows the result for three pixels 103 (triangles), 502 (boxes) and 835 (stars). In the upper panel the light leak signal as a function of orbit phase shows a maximum of 120 BU/s.

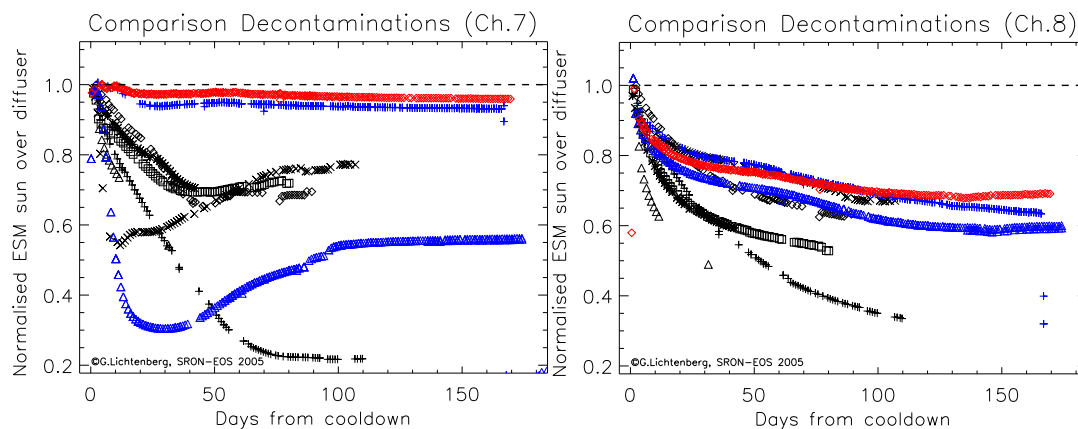


**Fig. 7.** Comparison of transmission behaviour after decontaminations. Daily updated plots are available at [http://www.sron.nl/index.php?option=com\\_content&task=view&id=322&Itemid=795](http://www.sron.nl/index.php?option=com_content&task=view&id=322&Itemid=795). Different symbols/colours mark different decontaminations. Shown is the transmission as a function of time since the cool down in days. The development after the decontaminations in December 2003 (crosses) and June 2004 (triangles) are marked blue. The development after the last decontamination in December 2004 is marked in red. All values are normalised to a measurement in January 2003 done shortly after a decontamination removed the ice. Left: channel 7. Right: channel 8.

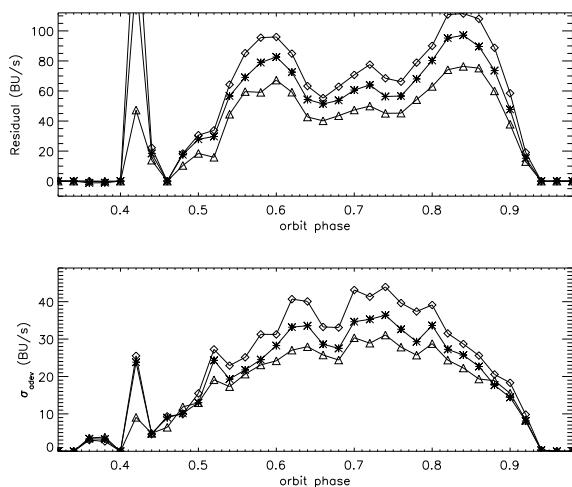


**Fig. 8.** Light Leak signal in channel 7 for pixels 103 (triangles), 502 (boxes) and 835 (stars). On the top panel the residual signal after being corrected for nonlinearity, dark measurement and spectral stray light is shown as a function of orbit phase, with phase zero defined as entry of the satellite into eclipse; sunrise occurs around orbit phase 0.4. The high peak seen at that orbit phase is caused by sunlight shining into the limb port and was expected. The bottom panel shows the mean absolute deviation for the same pixels from one month of data.

The signal is spectrally smooth and shows a systematic behaviour with orbit phase. However, the variation of the light leak signal from one observation to another is nearly as high as the light leak signal itself (see bottom panel of Fig. 8). This indicates that it is not only dependent on orbit phase, but probably also depends on the observation geometry and the presence of regions with high albedo, possibly caused by clouds. Up to now no set of parameters could be found

to fully characterise and correct the light leak with sufficient quality. While to the authors knowledge no retrieval has been attempted from channel 7 data<sup>6</sup>, it is very likely that most retrievals will be severely affected because of the magnitude of the signal caused by the light leak and its unpredictable behaviour. Clearly, further study to understand the cause of the light leak and to develop a correction is needed.

### 9.3 In-flight degradation monitoring

Only a short summary of the monitoring is given here. Details of the application of the monitoring to the calibration can be found in Slijkhuis (2000) and first results are described by Noël et al. (2003). Preliminary monitoring results can be found at <http://www-iup.physik.uni-bremen.de/sciamachy/LTM/LTM.html>. The correction of a given light path is done by comparing calibration and monitoring measurements to the same measurement at a chosen reference point in time. The results are the so-called m-factors, which will be incorporated in the Level 1 files and used in the calibration of the data. At the moment of this writing not enough Level 1 data of sufficient quality are available to do a proper monitoring, therefore a preliminary monitoring is done on the basis of Level 0 files. The results show that the UV channels 1 and 2 show an average degradation of the transmission of around 10% in the 3 years since launch. All other channels show a stable transmission with the exception of channels 7 and 8, where the ice layer leads to a gradual loss of transmission in between the decontaminations. A first investigation into the spectral dependency of the degradation seems to indicate that the channel edges and the regions with

<sup>6</sup>Possible products in this channel are temperature profiles, cloud fractions and CO<sub>2</sub> total columns.

a high polarisation sensitivity degrade the fastest. Degradation at the channel boundaries is expected. It is caused by a slow outgassing of the channel-separating dichroic mirrors. Studies to further investigate the degradation are planned.

## 10 Conclusions

In this paper we have described the basic concepts of the calibration of the SCIAMACHY instrument on-board ENVISAT. The calibration uses a combination of on-ground T/V and ambient measurements and a number of in-flight measurements. The individual calibration steps as well as problems encountered in the SCIAMACHY calibration have been discussed. The instrument itself has shown in general an excellent performance in the last 3 years. No major hardware problems were encountered and the in-orbit performance has not changed much with respect to the on-ground calibration. Notable exceptions are the ice deposition in channels 7 and 8, which is a problem that SCIAMACHY shares with two other instruments on the ENVISAT platform, the light leak in channel 7 and the growing number of degraded pixels in channel 7 and 8. Several errors in the on-ground calibration and the data processing were found in the last years, a large number of which will be corrected in the current update of the processing chain. After the update, the level 1 data will be significantly improved. Summarising, the following points can be made:

*Memory effect:* This effect is only seen in channels 1–5 and is an additive correction. Its effect on the retrieval is difficult to predict, but consecutive measured spectra of a highly variable scene and spectra with a high dynamic range are most likely to be affected. An updated version of the memory effect correction will be implemented during the current update of the operational processor to version 6.0.

*Non Linearity:* This effect is only seen in channels 6–8 and is an additive correction. The effect on the retrieval is expected to be minor. Only the retrieval of weakly absorbing trace gases is assumed to be affected. The non linearity correction will be implemented during the current update of the operational data processor.

*Bad and Dead Pixels:* Bad and dead pixels have to be masked out for retrievals, because they can ruin the retrieval of trace gases. Recently it has been discovered that the number of bad and dead pixels increases in-flight. The original calibration concept did not foresee a frequent update of the bad and dead pixel mask. Discussions between SRON and ESA have started on how to best implement a regular update of the mask into the operational processing.

*Dark correction:* The dark correction in channels 1–6 did not show strong variation since launch. In the channels 7 and 8 the dark correction changes every orbit, because of the ice layer growth. These channels need a dark correction de-

rived from an orbit measured as close as possible in time to the science measurement. Since March 2004 the operational processor (version 5.01) uses the closest available dark measurement in the dark correction.

*Orbital variation of darks:* Channel 8 shows a variation of the dark signal within one orbit caused by minute changes of the OBM temperature. The orbital variation has a significant impact on CH<sub>4</sub> retrievals and has to be taken into account in the retrieval. It will be implemented during the current update of the operational data processor.

*Changes caused by ice:* The growing ice layer in channels 7 and 8 leads to a decrease of the transmission. A lower signal-to-noise ratio in the reflectances is the result. A correction of the transmission is straight-forward, but not yet implemented in the operational processing. More detrimental to trace gas retrievals is the change of the instrument slit function caused by scattering of the incoming light by the ice layer. While SRON developed a slit function correction based on scenes with known trace gas content, it is not possible to implement this algorithm in the operational processing. An operational correction is not available at this moment. The operations of the instrument now include regular decontaminations to remove the ice.

*Light leak channel 7:* The spurious signal caused by the light leak can be as high as 120 BU/s. While some dependence of the signal on the orbit phase can be seen, the variation over time can be as high as the average light leak signal itself. Due to the erratic nature of the signal, no correction algorithm could be developed so far. The light leak will severely affect all retrievals in this channel.

*Spectral calibration:* SCIAMACHY is spectrally very stable with the possible exception of the channel overlaps, where a detailed investigation is needed.

*Stray light:* Apart from channel 1 the amount of spectral stray light is very low. A dedicated stray light correction for channel 1 is implemented in the processing and is able to reduce the stray light to around 1% of the incoming intensity for individual pixels. Spatial stray light was discovered in Limb observations. Investigation showed that the stray light is entering through the slit from regions outside the IFoV. The impact of the spatial stray light on retrievals and a possible correction has still to be investigated.

*Polarisation correction:* A conceptual limitation of the polarisation correction used in the calibration is the sensitivity to errors in the retrieved  $q$  and  $u$  values. Spectral features in the polarisation sensitivity  $\eta$  and  $\zeta$  will be introduced through the polarisation correction when the polarisation fractions are wrong. The size of the effect depends on the polarisation degree and the size of the error. Channels 1–3 are most sensitive to this kind of error. The currently implemented polarisation correction is not able to retrieve a physical value for  $u$  from the PMD D/PMD 45 combination, therefore a value

for  $u$  determined from the single scattering approximation is used in the determination of the correction factor  $c_{\text{pol}}$ . For some cases the polarisation fraction determined with PMD A in limb are unphysical. While a systematic study is missing, results show that the polarisation correction does not always remove all polarisation effects from the data. The correction was reviewed during the last year and improvement and bug fixes are implemented during the current update of the processor. After the implementation is finished, a new verification of the polarisation correction is planned.

*Radiometric calibration:* The basis of most retrievals is the ratio of the radiance reflected from the Earth's atmosphere to the solar irradiation. SCIAMACHY can measure the solar irradiation with two diffusers, mounted on the ESM and the ASM. Preliminary studies showed that the ASM diffuser is more suitable for DOAS type retrievals than the ESM diffuser. The ASM diffuser is not radiometrically calibrated, while the ESM diffuser is. However, the original radiometric calibration produced solar spectra that were up to 10% too high and reflectances that were 15–20% too low. Newly calculated radiometric calibration data reduce this offset, producing reflectances that are good within 5% in the tested wavelength range, but they also introduce spectral features. Usually retrievals that need an accurate reflectance are not as sensitive to spectral features as DOAS type retrievals, but it has to be investigated, if this is a valid assumption for the introduced spectral features. The new radiometric calibration data are incorporated in the current update and investigations on how to improve the radiometric further are going on.

*Acknowledgements.* We wish to thank all members of the Calibration Tiger Team, especially J. Frerick (ESA), K. Gerilowski (IfE), G. Otter (TNO) for fruitful discussions about calibration issues and for their continuous work to improve the calibration of SCIAMACHY.

SCIAMACHY is a joint project of the German Space Agency DLR and the Dutch Space Agency NIVR with contribution of the Belgian Space Agency BUSOC.

Data were provided by the European Space Agency.

Edited by: U. Platt

## References

- Aben, I., E., Eisinger, M., H., Snel, R., and Tanzi, C.: GDAQI Final Report, TN-GDAQI-003SR/2000, Tech. rep., ESA/ESRIN, 2000.
- Aberle, B., Balzer, W., von Barga, A., Hegels, E., Loyola, D., and Spurr, R.: GOME Level 0 to 1 Algorithms Description (ERTN-DLR-GO-0022), Tech. Rep. 5a, DLR, <http://atmos.caf.dlr.de/cgi-bin/h.cgi?page=projdocs>, 2000.
- Acarreta, R. J. and Stammes, P.: Calibration Comparison between SCIAMACHY and MERIS onboard ENVISAT, IEEE Geosc. Rem. Sens. Lett., 2, 31–35, 2005.
- Ahlers, B.: Investigation of the sun irradiance offset in comparison with standard sun irradiances (TPD-SCIA-PhE-TN-10), Tech. rep., TNO, 2003.
- Ahlers, B.: Comparison of SLS and WLS calibration measurements on-ground and in-flight (TPD-SCIA-PhE-TN-013), Tech. rep., TNO, 2004a.
- Ahlers, B.: Performance verification of spectral shift by vignetting of SLS (TPD-SCIA-PhE-015), Tech. rep., TNO, 2004b.
- Ahlers, B., Bazalgette Correges-Lacoste, G., Schrijvers, C., and Brug, H.: In-orbit detection of spectral features in SCIAMACHY, in: Sensors, Systems, and Next Generation Satellites VIII, vol. 5570 of Proc. SPIE, pp. 401–410, 2004.
- Akima, H.: A new method of interpolation and smooth curve fitting based on local procedures, J. ACM, 17, 589–602, 1970.
- Bovensmann, H., Burrows, J. P., Buchwitz, M., Frerick, J., Noël, S., Rozanov, V. V., Chance, K. V., and Goede, A. P. H.: SCIAMACHY: Mission objectives and Measurement Modes, Atmos. Sci., 56, 127–150, 1999.
- Buchwitz, M., de Beek, R., Noël, S., Burrows, J. P., Bovensmann, H., Bremer, H., Bergamaschi, P., Körner, S., and Heimann, M.: Carbon monoxide, methane and carbon dioxide columns retrieved from SCIAMACHY by WFM-DOAS: year 2003 initial data set, Atmos. Chem. Phys., 5, 3313–3329, 2005, <http://www.atmos-chem-phys.net/5/3313/2005/>.
- Burrows, J. P., Weber, M., Buchwitz, M., Rozanov, V., Ladstätter-Weißmayer, A., Richter, A., Debeek, R., Hoogen, R., Bramstedt, K., Eichmann, K.-U., Eisinger, M., and Perner, D.: The Global Ozone Monitoring Experiment (GOME): Mission Concept and First Scientific Results., J. Atmos. Sci., 56, 151–175, 1999.
- Coulson, K. L.: Polarisation and intensity of Light in the atmosphere, A. Deepak, Hampton, Va., USA, 1988.
- de Beek, R. and Bovensmann, H.: Impact of SCIAMACHY Diffuser Spectral Characteristics on Level 1-2 DOAS Products, Tech. rep., IfE, 2000.
- Falk, W. R.: Data Reduction from Experimental Histograms, Nuclear Instruments and methods in Physics Research, 220, 473–478, 1984.
- Frankenberg, C., Platt, U., and Wagner, T.: Retrieval of CO from SCIAMACHY onboard ENVISAT: detection of strongly polluted areas and seasonal patterns in global CO abundances, Atmos. Chem. Phys., 5, 1639–1644, 2005, <http://www.atmos-chem-phys.net/5/1639/2005/>.
- Frerick, J.: How to generate phase shift corrected greek key data (IFE-TN-211299), Tech. rep., IfE, 1999.
- Gloudemans, A. M. S., Schrijver, H., Kleipool, Q., van den Broek, M. M. P., Straume, A., Lichtenberg, G., van Hees, R. M., Aben, I., and Meirink, J. F.: The impact of SCIAMACHY near-infrared instrument calibration on CH<sub>4</sub> and CO total columns, Atmos. Chem. Phys., 5, 2369–2383, 2005, <http://www.atmos-chem-phys.net/5/2369/2005/>.
- Grundy, W. M. and Schmitt, B.: The Temperature-dependent Near-Infrared Absorption Spectrum of Hexagonal H<sub>2</sub>O ice, J. Geophys. Res. E, 103, 25 809–25 822, 1998.
- Gurlit, W., Bösch, H., Bovensmann, H., Burrows, J. P., Butz, A., Camy-Peyret, C., Dorf, M., Gerilowski, K., Lindner, A., Noël, S., Platt, U., Weidner, F., and Pfeilsticker, K.: The UV-A and visible solar irradiance spectrum: inter-comparison of absolutely calibrated, spectrally medium resolution solar irradiance spectra

- from balloon- and satellite-borne measurements, *Atmos. Chem. Phys.*, 5, 1879–1890, 2005, <http://www.atmos-chem-phys.net/5/1879/2005/>.
- Hansen, J. E. and Travis, L. D.: Light scattering in planetary atmospheres, *Space Sci. Rev.*, 16, 527–610, 1974.
- Hasekamp, O. P., Landgraf, J., and van Oss, R.: The need of polarization modeling for ozone profile retrieval from backscattered sunlight, *J. Geophys. Res. D (Atmospheres)*, pp. 13, 2002.
- Hoogeveen, R. W. M., van der A, R. J., and Goede, A. P. H.: Extended wavelength InGaAs infrared (1.0–2.4  $\mu\text{m}$ ) detector arrays on SCIAMACHY for space-based spectrometry of the Earth atmosphere, *Infrared Phys. Technol.*, 42, 1–16, 2001.
- Kleipool, Q.: SCIAMACHY SODAP; Objective 38: Leakage current versus temperature (SRON-SCIA-PhE-RP-006), Tech. rep., SRON, [http://www.sron.nl/~rienk/update\\_sronserver/docs/obj38\\_lcvstemp.ps](http://www.sron.nl/~rienk/update_sronserver/docs/obj38_lcvstemp.ps), 2002.
- Kleipool, Q.: SCIAMACHY: Recalculation of OPTEC 5 Non-Linearity (SRON-SCIA-PhE-RP-013), Tech. rep., SRON, [http://www.sron.nl/~rienk/update\\_sronserver/docs/rp013.ps.gz](http://www.sron.nl/~rienk/update_sronserver/docs/rp013.ps.gz), 2003.
- Kleipool, Q. L., Jongma, R. T., Gloudemans, A. M. S., Schrijver, H., Lichtenberg, G. F., and van Hees, R. M.: In-flight proton-induced radiation damage to SCIAMACHY's extended-wavelength InGaAs near-infrared detectors, *Infrared Phys. Technol.*, <http://www.sciencedirect.com/science/article/B6TJ9-4M1D0G5-1/2/f8607b5924aa52ef5216c13faf78935f>, accepted, doi:10.1016/j.infrared.2006.08.001, 2006.
- Kurucz, R.: The solar spectrum: atlases and line identifications, in: *Laboratory and Astronomical High Resolution Spectra*, edited by: Sauval, A., Blomme, R., and Grevesse, N., of *Astron. Soc. of the Pacific Conf. Series*, 81, 17–31, 1995.
- Latter, B. G., Siddans, R., and Kerridge, B. J.: Intercomparison of Reflectances Observed by SCIAMACHY, GOME, AATSR and ATSR-2, EGS – AGU – EUG Joint Assembly, Abstracts from the meeting held in Nice, France, 6–11 April 2003, abstract #11451, pp. 11 451, 2003.
- Lichtenberg, G.: SCIAMACHY channel 1-5 Memory Effect I: Key data implementation and in-flight measurements (SRON-SCIA-PhE-RP-11, issue 2), Tech. rep., SRON, [http://www.sron.nl/~rienk/update\\_sronserver/docs/memory\\_effect\\_sronrpI.pdf](http://www.sron.nl/~rienk/update_sronserver/docs/memory_effect_sronrpI.pdf), 2003.
- McLinden, C. A., McConnell, J. C., Griffioen, E., and McElroy, C. T.: A vector radiative-transfer model for the Odin/OSIRIS project, *Can. J. Phys.*, 80, 375, 2002.
- Noël, S., Bovensmann, H., Wuttke, M. W., Burrows, J. P., Gottwald, M., Krieg, E., Goede, A. P. H., and Muller, C.: Nadir, limb, and occultation measurements with SCIAMACHY, *Adv. Space Res.*, 29, 1819–1824, 2002.
- Noël, S., Bovensmann, H., Skupin, J., Wuttke, M. W., Burrows, J. P., Gottwald, M., and Krieg, E.: The SCIAMACHY calibration/monitoring concept and first results, *Adv. Space Res.*, 32, 2123–2128, 2003.
- Noël, S.: Determination of Correction Factors for SCIAMACHY Radiances and Irradiances (IFE-SCIA-SN-20040618\_IrrRadCorrection, issue 5.1), Tech. rep., IFE, [http://www.iup.physik.uni-bremen.de/sciamachy/SCIA.CAL/rad\\_cal.html](http://www.iup.physik.uni-bremen.de/sciamachy/SCIA.CAL/rad_cal.html), 2005.
- Perron, G.: MIPAS Level 1b Changes & Status, presentation given at the ESA ACVE–2 workshop, <http://envisat.esa.int/workshops/acve2/>, 2004.
- Platt, U.: Differential optical absorption spectroscopy (DOAS), in: *Air Monitoring by Spectroscopic Techniques*, edited by M. Siegrist, vol. 127 of *Chemical Analysis Series*, pp. 27–84, John Wiley and Sons, New York, 1994.
- Schrijvers, C.: Relative BRDF (BRDF\_rel) keydata based on in-flight measurements (TPD-SCIA-PhE-TN-012), Tech. rep., TNO, 2004.
- Schutgens, N. A. J., Tilstra, L. G., Stammes, P., and Bréon, F.-M.: On the relationship between Stokes parameters Q and U of atmospheric ultraviolet/visible/near-infrared radiation, *J. Geophys. Res. D (Atmospheres)*, 109, D09 205, doi:10.1029/2003JD004081, 2004.
- Sierk, B.: Study of the impact of ASM diffuser solar spectra on the retrieval of minor trace gases (SCIAMACHY Lv0-1 masterplan workpackage 2.11.1.2.) (IFE-TN-19062003-MB), Tech. rep., IFE, 2003.
- Skupin, J., Noel, S., Wuttke, M. W., Bovensmann, H., Burrows, J. P., Hoogeveen, R., Kleipool, Q., and Lichtenberg, G.: In-flight calibration of the SCIAMACHY solar irradiance spectrum, *Adv. Space Res.*, 32, 2129–2134, 2003.
- Slijkhuis, S.: ENVISAT-1 SCIAMACHY Level 0 to 1c Processing, Algorithm Theoretical Basis Document, issue 2 (ENV-ATB-DLR-SCIA-0041), Tech. rep., DLR, <http://atmos.af.op.dlr.de/cgi-bin/h.cgi?page=projdocs>, 2000.
- Smith, D. L.: AATSR instrument performance verification and optimisation, in: *Proceedings of the ENVISAT calibration review (Special publication SP 520)*, edited by: Sawaya-Lacoste, H., <http://envisat.esa.int/calval/proceedings/>, 2002.
- Solomon, S., Schmeltekopf, A. L., and Sanders, R. W.: On the interpretation of zenith sky absorption measurements, *J. Geophys. Res.*, 92, 8311–8319, 1987.
- Tilstra, L. G. and Stammes, P.: Spectral calibration inconsistency found in the overlap region between channels 2 and 3, Tech. rep., KNMI, <http://www.knmi.nl/~tilstra>, 2004.
- Tilstra, L. G. and Stammes, P.: Alternative polarisation retrieval for SCIAMACHY in the ultraviolet, *Atmos. Chem. Phys.*, 5, 2009–2107, 2005, <http://www.atmos-chem-phys.net/5/2009/2005/>.
- Tilstra, L. G., de Graaf, M., and Stammes, P.: Verification of SCIAMACHY'S radiometric calibration using GOME colocated Reflectance data, Tech. rep., KNMI, <http://www.knmi.nl/~tilstra>, 2003.
- Tilstra, L. G., van Soest, G., Acarreta, J. R., and Stammes, P.: Verification of the radiometric calibration of SCIAMACHY in the UV for two alternative key data sets, Tech. rep., KNMI, <http://www.knmi.nl/~tilstra>, 2004.
- Tilstra, L. G., Acarreta, J. R., and Stammes, P.: Jumps in the SCIAMACHY Level-1c reflectance spectrum due to failing polarisation correction, in: *Proceedings ENVISAT/ERS symposium 2004*, Salzburg ESA-SP-572, edited by: Lacoste, H. and Ouwehand, L., ESA, 2005.
- van Soest, G.: Investigation of SCIAMACHY Limb stray light (SRON-EOS-RP-05-006), Tech. rep., SRON, [http://www.sron.nl/~rienk/update\\_sronserver/docs/invlimbstray.pdf](http://www.sron.nl/~rienk/update_sronserver/docs/invlimbstray.pdf), 2005.
- van Soest, G., Tilstra, L. G., and Stammes, P.: Large-scale validation of SCIAMACHY reflectance in the ultraviolet, *Atmos. Chem. Phys.*, 5, 2171–2180, 2005, <http://www.atmos-chem-phys.net/5/2171/2005/>.